# Lattice calculation of heavy-light decay constants with two flavors of dynamical quarks

C. Bernard,[1] S. Datta,[2,3] T. DeGrand,[4] C. DeTar,[5] Steven Gottlieb,[2] Urs M. Heller,[6] C. McNeile,[7] K. Orginos,[8] R. Sugar,[9] and D. Toussaint[10]

(MILC Collaboration)

[1]*Washington University, St. Louis, Missouri 63130*
[2]*Indiana University, Bloomington, Indiana 47405*
[3]*Fakultät für Physik, Universität Bielefeld, D-33615 Bielefeld, Germany*
[4]*University of Colorado, Boulder, Colorado 80309*
[5]*University of Utah, Salt Lake City, Utah 84112*
[6]*CSIT, The Florida State University, Tallahassee, Florida 32306-4120*
[7]*Department of Mathematical Sciences, University of Liverpool, Liverpool, L69 3BX, United Kingdom*
[8]*RIKEN BNL Research Center, Upton, New York 11973*
[9]*University of California, Santa Barbara, California 93106*
[10]*University of Arizona, Tucson, Arizona 85721*

(Received 19 June 2002; published 12 November 2002)

We present results for $f_B$, $f_{B_s}$, $f_D$, $f_{D_s}$ and their ratios in the presence of two flavors of light sea quarks ($N_f=2$). We use Wilson light valence quarks and Wilson and static heavy valence quarks; the sea quarks are simulated with staggered fermions. Additional quenched simulations with nonperturbatively improved clover fermions allow us to improve our control of the continuum extrapolation. For our central values the masses of the sea quarks are not extrapolated to the physical $u$, $d$ masses; that is, the central values are ''partially quenched.'' A calculation using ''fat-link clover'' valence fermions is also discussed but is not included in our final results. We find, for example, $f_B=190(7)(^{+24}_{-17})(^{+11}_{-2})(^{+8}_{-0})$ MeV, $f_{B_s}/f_B=1.16(1)(2)(2)(^{+4}_{-0})$, $f_{D_s}=241(5)(^{+27}_{-26})(^{+9}_{-4})(^{+5}_{-0})$ MeV, and $f_B/f_{D_s}=0.79(2)(^{+5}_{-4})(3)(^{+5}_{-0})$, where in each case the first error is statistical and the remaining three are systematic: the error within the partially quenched $N_f=2$ approximation, the error due to the missing strange sea quark and to partial quenching, and an estimate of the effects of chiral logarithms at small quark mass. The last error, though quite significant in decay constant ratios, appears to be smaller than has been recently suggested by Kronfeld and Ryan, and Yamada. We emphasize, however, that as in other lattice computations to date, the lattice $u,d$ quark masses are not very light and chiral log effects may not be fully under control.

DOI: 10.1103/PhysRevD.66.094501 PACS number(s): 12.38.Gc, 12.15.Hh, 13.20.−v

## I. INTRODUCTION

Accurate values for the leptonic decay constants of $B$ and $B_s$ mesons are crucial for interpreting experimental measurements of $B$-$\bar{B}$ mixing and bounds on, or future measurements of, $B_s$-$\bar{B}_s$ mixing. Knowledge of the decay constants (coupled with knowledge of the corresponding $B$ parameters) makes possible a determination of the Cabibbo-Kobayashi-Maskawa (CKM) elements $V_{td}$ and $V_{ts}$ from these experiments.

In the $D$-meson sector, CLEO-c will measure leptonic decay rates at the 3–4 % level [1]. Assuming 3-generation unitarity, this translates into determinations of $f_{D_s}$ and $f_D$ with roughly 2% accuracy. Coupled with accurate theoretical computations of ratios such as $f_B/f_{D_s}$, this will provide crucial information about the $B$ sector. In addition, if computations of the $D$ and $D_s$ decay constants themselves can be performed at the few percent level, the experiments will directly determine $V_{cs}$ and $V_{cd}$ with similar precision.

At least in principle, lattice QCD offers a means to compute quantities such as $f_B$ or $f_B/f_{D_s}$ with control over all sources of systematic error. Here, we present a computation by the MILC Collaboration of the decay constants $f_B$, $f_{B_s}$, $f_D$, $f_{D_s}$, and their ratios. We take into account the effects of virtual quark loops from two light flavors of sea quarks; i.e., we have two ''dynamical quarks.'' Additional discussion and preliminary results for the dynamical calculation can be found in Refs. [2,3]. Our earlier work, which focused on the quenched approximation and used dynamical configurations only for an estimate of the quenching errors, appeared in [4], with further details in [5].

This paper is organized as follows. Our lattice formalism is presented in Sec. II. We discuss the Fermilab approach to heavy quarks on the lattices [6], and explain how we adapt it to Wilson and nonperturbatively improved [7] clover quarks. We also explain our use of perturbative renormalization and the choice of scale (''$q^*$'').

Section III gives the lattice computational details. We discuss the generation of configurations, the evaluation of quark propagators for Wilson, clover, and static quarks, and various aspects of the analysis, including fitting and extrapolation. The most significant open issue here involves the effect of chiral logarithms on the light quark mass extrapolations. In important recent work, Kronfeld and Ryan [8] and Yamada [9] (building on work of the JLQCD Collaboration [10]) have argued that standard linear or quadratic extrapolations from typical lattice light quark masses miss the logarithms at

 

low mass and drastically underestimate such quantities as $f_{B_s}/f_B$. Since the quark masses available to the present calculation are of this typical size, it is imperative that we estimate the chiral logarithm effects as best we can. We devise a method to estimate, at least crudely, such effects. The method is based on the extrapolation of the ratio of the light-light to the heavy-light decay constant.

In Sec. IV we reexamine the quenched approximation. The dominant source of systematic error in our previous quenched computation [4] was the continuum extrapolation. Two new features of the current analysis have significantly reduced that error: (i) new running with both Wilson and clover quarks and (ii) a new central value for the scale $q^*$ for the heavy-light axial current [11].

We then turn to the dynamical quark data in Sec. V. The improved control over discretization errors in the quenched approximation gives us more confidence in the central value and errors deduced from the continuum extrapolation of our dynamical quark data. Other sources of systematic error, including the chiral extrapolation, higher order perturbation theory, and the effects of partial quenching are also discussed in detail. Finally we clarify the effects of ''fat-link'' fermions using some new test runs in the quenched case. These shed light on why the preliminary values for heavy-light decay constants with fat-link fermions on dynamical configurations were anomalously low [12].

Our conclusions and the outlook for reducing the main systematic uncertainties are discussed in Sec. VI. We describe work in progress that addresses the outstanding issues in the chiral and continuum extrapolations.

The computation presented in this paper is rather complicated: we use several different actions, operators, renormalizations, fitting techniques, and extrapolations. Part of the reason for this is that the simulations with dynamical quarks are extremely demanding computationally and therefore have taken years to complete. During that time, as our understanding of the physics and analysis issues grew, our methods evolved. The variety of methods used does have one important virtue: it allows us to estimate many of the systematic effects in a direct way.

## II. FORMALISM

In a groundbreaking paper [6], El-Khadra, Kronfeld and Mackenzie (EKM) show that one can make sense of heavy Wilson-like[1] fermions on the lattice even when $am_Q \gtrsim 1$, where $a$ and $m_Q$ are the lattice spacing and heavy quark mass, respectively. Indeed, in the nonrelativistic limit $m_Q \gg \Lambda_{QCD}$, they show that the effective Hamiltonian has the form (after Foldy-Wouthuysen-Tani transformation)

$$H = \overline{Q}\left( M_1 + \gamma_0 A_0 - \frac{\vec{D}^2}{2M_2} - \frac{i\vec{\Sigma}\cdot\vec{B}}{2M_3}\right) Q + \mathcal{O}(1/m_Q^2), \quad (1)$$

where $Q$ is the effective heavy quark field, $\vec{D}$ is the spatial covariant derivative, $\vec{B}$ is the chromomagnetic field, $\vec{\Sigma}$ are the Pauli matrices, and $m_Q$ is a generic heavy quark mass. The masses $M_1$, $M_2$, and $M_3$ are particular functions of the bare heavy quark mass $am_0$ that depend on the quark action. Here $m_0$ is given by

$$am_0 = \frac{1}{2\kappa_Q} - \frac{1}{2\kappa_c}, \quad (2)$$

where $\kappa_Q$ is the heavy quark hopping parameter and $\kappa_c$ is its critical value.[2] The ''pole mass,'' $M_1$, controls the exponential decay of the zero-momentum propagator in Euclidean time, but is just an additive constant in bound state energies. The nontrivial physics of a heavy quark in a heavy-light bound state is controlled at this order by the ''kinetic mass,'' $M_2$, which fixes the heavy-quark energy-momentum dispersion relation, and the ''magnetic mass,'' $M_3$, which governs chromomagnetic effects, such as hyperfine splittings.

For computations of heavy-light decay constants, one also needs to know how the lattice axial current, $\overline{q}\gamma_0\gamma_5 Q$, renormalizes. At tree level but through order $(1/m_Q)$, EKM show that the renormalization is given simply by the replacement, $Q \to Q_I$, where the tree-level improved field is

$$Q_I(x) = \sqrt{2\kappa_Q e^{aM_1}}[1 + ad_1\vec{\gamma}\cdot\vec{D}]Q(x), \quad (3)$$

with $d_1$ another function of $am_0$. We have included the standard $\sqrt{2\kappa_Q}$ factor needed to go from lattice-normalized to continuum-normalized fields.

At tree level, one has

$$aM_1 = \ln(1+am_0),$$

$$aM_2 = \frac{am_0(1+am_0)(2+am_0)}{2+4am_0+(am_0)^2} = \frac{e^{aM_1}\sinh(aM_1)}{1+\sinh(aM_1)},$$

$$aM_3 = \frac{am_0(1+am_0)(2+am_0)}{2(1+am_0)+c_{SW}am_0(2+am_0)},$$

$$d_1 = \frac{am_0}{2(1+am_0)(2+am_0)}, \quad (4)$$

where $c_{SW}$ is the coefficient of the clover term.

[1] ''Wilson-like'' means that the fermion action includes the naive discretization of the Dirac equation plus a Wilson term to remove doublers. There may be further additional correction terms to reduce lattice artifacts. Standard Wilson fermions as well as ''clover'' fermions [13] fall into this class.

[2] We assume throughout this paper that the spatial and temporal hopping parameters are chosen equal, that the Wilson parameter $r = 1$, and that the spatial and temporal parts of the clover term, if present, have equal coefficients. This is not the complete generality of Ref. [6], but is sufficient for our purposes.

A large fraction of the one-loop corrections to Eq. (4) can be included with tadpole renormalization [14]. We use $\kappa_c$ to define the mean field value, $u_0$, of the gauge link: $u_0 \equiv 1/(8\kappa_c)$. Absorbing $u_0$ into $\kappa$ gives a tadpole-improved hopping parameter, $\tilde{\kappa}$, and bare mass, $\tilde{m}_0$:

$$\tilde{\kappa} \equiv u_0 \kappa = \frac{\kappa}{8\kappa_c}, \quad \tilde{\kappa}_c = 1/8$$

$$a\tilde{m}_0 \equiv am_0/u_0 = \frac{1}{2\tilde{\kappa}} - \frac{1}{2\tilde{\kappa}_c} = 4\frac{\kappa_c}{\kappa} - 4. \tag{5}$$

We denote the tadpole-improved versions of the quantities in Eq. (4) by $\tilde{M}_1$, $\tilde{M}_2$, $\tilde{M}_3$, and $\tilde{d}_1$. They are found simply by replacing $m_0 \to \tilde{m}_0$. Similarly, the tadpole-improved version of Eq. (3) is

$$\begin{aligned}\tilde{Q}_I(x) &= \sqrt{2\kappa_Q u_0 e^{a\tilde{M}_1}}[1 + a\tilde{d}_1 \vec{\gamma}\cdot\vec{D}]Q(x) \\ &= \sqrt{1 - \frac{3\kappa_Q}{4\kappa_c}}[1 + a\tilde{d}_1 \vec{\gamma}\cdot\vec{D}]Q(x).\end{aligned} \tag{6}$$

For some applications, the $\tilde{d}_1$ term here may be neglected. It is therefore convenient also to define

$$\tilde{Q}_I^0(x) \equiv \sqrt{1 - \frac{3\kappa_Q}{4\kappa_c}}Q(x). \tag{7}$$

We take the physical mass of our lattice heavy-light mesons to be the meson kinetic mass, $M_{Qq,2}$. Although $M_{Qq,2}$ could be determined directly from the meson dispersion relation, that would require the computation of meson propagators with nonzero momenta, which in any case are rather noisy. Instead we define $M_{Qq,2}$ by [15]

$$M_{Qq,2} = M_{Qq,1} + \tilde{M}_2 - \tilde{M}_1, \tag{8}$$

where $M_{Qq,1}$ is the pole mass of the meson determined on the lattice, and $\tilde{M}_2$ and $\tilde{M}_1$ refer to the heavy quark, $Q$. The UKQCD Collaboration, in Fig. 8 of Ref. [16], compares the kinetic meson mass determined by the dispersion relation with that given by Eq. (8) (but without tadpole improvement). The agreement is good, and would in fact be still better if the tadpole improved version were used.

### A. Wilson fermions

For Wilson fermions ($c_{SW}=0$), the magnetic mass $M_3$ is not equal to the kinetic mass $M_2$, even at tree level. As discussed in Refs. [17] and [4], this produces an error at fixed $a$ of $\mathcal{O}[(c_{mag}-1)\Lambda_{QCD}/M_{Qq}]$, where $c_{mag} \equiv M_2/M_3$. Hence there is little point in keeping the $\tilde{d}_1$ term in Eq. (6), which is also of $\mathcal{O}(\Lambda_{QCD}/M_{Qq})$. [Indeed, keeping such terms without including at least the $\mathcal{O}(g^2)$ perturbative corrections to them is likely to increase the systematic error [3].] We thus set $\tilde{d}_1 = 0$ in the Wilson case and use Eq. (7).

The 1-loop mass-dependent perturbative matching for the heavy-light axial vector current has been calculated by Kuramashi [18]. Since we include tadpole renormalization for both the heavy and light quarks through Eq. (7) (with $\tilde{d}_1 = 0$), we adjust the result to reflect our choice of $\kappa_c$ to define the mean link (Ref. [18] uses the Feynman-gauge link). The continuum contribution to the matching generates a logarithm of the heavy quark mass. In [18], this is taken as $\log M_1$. Since we take $M_2$ as the physical mass, we also adjust the result of [18] to replace $M_1$ with $M_2$ in the logarithm.

Additional issues for perturbative matching are the definition of the coupling constant and the scale at which it is evaluated. We use the coupling $\alpha_V$, whose value at scale $3.4018/a$ is defined in terms of the plaquette [14,19]. It has become standard to evaluate the coupling at the Lepage-Mackenzie scale $q^*$ [14], defined by

$$\log((q^*)^2) = \frac{\int d^4q I(q)\log(q^2)}{\int d^4q I(q)}, \tag{9}$$

where $I(q)$ is the complete integrand for the quantity of interest. In other words, the 1-loop axial vector current renormalization constant, $Z_A$, is given by $Z_A = 1 + \alpha_V(q^*)C_F z_A/(4\pi)$, where $C_F$ is the quadratic Casimir and $z_A \equiv \int d^4q I(q)$. Here, we need $Z_A$ in three cases (light-light, static-light, and heavy-light), which we denote by $Z_A^{\rm qq}$, $Z_A^{\rm Statq}$, and $Z_A^{\rm KUR}$, respectively, where KUR emphasizes that we are talking about the heavy-light renormalization constant computed by Kuramashi [18]. We adopt corresponding notation for $z_A$ and $I$.

Unfortunately, at the time the analysis described here was performed, $q^*$ for $Z_A^{\rm KUR}$ had not been determined [20]. For $Z_A^{\rm qq}$ with $\kappa_c$-tadpole improvement, $q^* = 2.32/a$ [21], which we use here when fixing the scale through $f_\pi$. For $Z_A^{\rm Statq}$ with plaquette tadpole improvement, Hernandez and Hill [22] found $q^* = 2.18/a$. Since the light-light and static-light values of $q^*$ were so close, it was argued in [4] that either could be used in the heavy-light case, and in fact the light-light value $q^* = 2.32/a$ was chosen for the standard computation (central value).

Recently, Bernard and DeGrand [11] have repeated the Hernandez and Hill computation. They find a significantly different value of $q^*$ for the $\kappa_c$-tadpole-improved $Z_A^{\rm Statq}$. Their result depends on the heavy-light mass, which enters through the continuum part of the matching. However the mass dependence is rather weak over the range of masses used in the current numerical work, and it is therefore adequate to use an average value $q^* \approx 1.43/a$. Since Ref. [11] has not yet appeared, it may be helpful to summarize here the reasons for the disagreement with Ref. [22].

First of all, Ref. [22] sets to zero certain parts of the lattice integrand whose contributions to the matching vanish by contour integration. This is a standard procedure [23] for evaluating integrals involving a static quark propagator. However, such integrals do not vanish when the integrand is

first multiplied by $\log(q^2)$, as in Eq. (9). Bernard and DeGrand argue that it is incorrect to discard parts of the integrand unless their contributions to both the numerator and denominator of Eq. (9) vanish.

Secondly, there are ''constant'' terms in the matching coming from the dimensionally regularized continuum integrals. Hernandez and Hill treat these as constant over the 4-dimensional Brillouin zone. Similarly, the $\log(am_Q)$ term in $Z_A^{\rm Statq}$, which comes from both continuum and lattice integrals, is set to zero in [22] by the choice $a=1/m_Q$. In contrast, Ref. [11] keeps the full continuum integrands as well as the full lattice integrands. This does introduce a small amount of arbitrariness: the dimensionally regulated continuum integrals must be replaced by finite, subtracted 4-dimensional integrals, and there is some freedom in how the subtraction is done. However, as long as the subtraction is ''reasonable,'' the arbitrariness in $q^*$ is small. If we accept the results of Ref. [11], then $q^*$ for $Z_A^{\rm Statq}$ is no longer very close to $q^*$ for $Z_A^{\rm qq}$. Instead, we take the static-light $q^* \approx 1.43/a$ for $Z_A^{\rm KUR}$. Since $am_B$ is quite large on our lattices ($\approx 1.2$ to 4), we believe this is a reasonable choice. Of course, it is always necessary to consider a range of $q^*$ to estimate perturbative errors, and the range we pick (see Sec. IV) includes the light-light $q^*$, as well as the values in Ref. [20].

Summarizing the results of this section, we may express the 0th component of our renormalized heavy-light current as

$$A_0^{\rm KUR} = Z_A^{\rm KUR}(q^*)\bar{\tilde{q}}_I^0 \gamma_0\gamma_5 \tilde{Q}_I^0, \tag{10}$$

with $q^*=1.43/a$, with $\tilde{Q}_I^0$ given by Eq. (7), and with a corresponding expression for the tadpole improved light quark field, $\tilde{q}_I^0$. For convenience, we also use Eq. (10) for the light-light pseudoscalars (''pions''), even though the mass dependence of Ref. [18] is negligible in that case. We take $q^*=2.32/a$ [21] for light-light renormalization.

The errors in our heavy-light Wilson calculation are formally $\mathcal{O}(a\Lambda_{QCD})$ and $\mathcal{O}(\alpha_V^2)$. Note that, in the Fermilab formalism, one should think of these errors as multiplied by an arbitrary [but presumably $\mathcal{O}(1)$] function of $aM_Q$, since we are working to all orders in $aM_Q$. Thus the dependence on $a$ is in general complicated. An example of such complicated behavior is the difference between lattice chromomagnetic effects, which go like $a\Lambda_{QCD}/(aM_3)$, and the desired behavior $a\Lambda_{QCD}/(aM_2)$ [see Eq. (4)]. Of course, in the truly asymptotic regime where $aM_Q \ll 1$, the leading errors are indeed linear in $a$, but this region is not currently accessible in practical calculations.

In the static-light case, we have

$$A_0^{\rm STAT} = Z_A^{\rm STAT}(q^*)\bar{\tilde{q}}_I^0 \gamma_0\gamma_5 h, \tag{11}$$

where $h$ is the static quark field, $Z_A^{\rm STAT}$ is the one-loop renormalization constant for the static-light current [23,24] with tadpole improvement, and $q^*=1.43/a$.

### B. Nonperturbative clover fermions

For our computations with clover fermions, we take the clover coefficient $c_{SW}$ calculated nonperturbatively by the ALPHA Collaboration [7]. The 0th component of the renormalized, improved [through $\mathcal{O}(a)$] light-light axial vector current (which is needed here to set the scale with $f_\pi$) is then

$$A_0^{\rm NP} = Z_A^{\rm NP}\sqrt{4\kappa_{q_1}\kappa_{q_2}}(1+b_A a\bar{m}_0)[A_0 + c_A a\partial_0 P_5],$$

$$A_0 = \bar{q}_1\gamma_0\gamma_5 q_2; \quad P_5 = \bar{q}_1\gamma_5 q_2, \tag{12}$$

where $\kappa_{q_1}$, $\kappa_{q_2}$ are the hopping parameters of the light quarks, and $\bar{m}_0 = (m_{q_1,0}+m_{q_2,0})/2$ is their average bare mass. $Z_A^{\rm NP}$ and $c_A$ are the nonperturbative values given in [7]. The coefficient $b_A$ has not been determined nonperturbatively by the ALPHA Collaboration, although the difference $b_A - b_P$ has [25]. Bhattacharya *et al.* [26] have determined $b_A$ at $\beta=6.0$ and 6.2, but not at $\beta=6.15$, which is one of the couplings used here. Our $b_A$ is therefore taken from perturbation theory [27], but with coupling $\alpha_V(q^*)$, with $q^*$ chosen as the value ($\cong 1/a$) that produces the nonperturbative result [7] for the similar quantity $b_V$. This gives $b_A=1.47$ at $\beta=6.15$ and 1.42 at $\beta=6.0$. In the systematic error analysis, we allow $b_A$ to vary over a range of values[3] (see Sec. IV).

For chiral extrapolations, our canonical procedure (see Sec. III D) for both Wilson and clover quarks is to use the kinetic quark mass $aM_2$ [Eq. (4)] as the independent variable. Through $\mathcal{O}(a)$, this is equivalent to the clover ''improved quark mass,'' $a\tilde{m}_q = am_0(1+b_m am_0)$, with the choice $b_m=-0.5$. A nonperturbative determination by the ALPHA Collaboration [25] gives instead $b_m \approx -0.709$ at $\beta=6.0$ and $b_m \approx -0.695$ at $\beta=6.15$; while boosted perturbation theory with the result of Ref. [27] gives $b_m=-0.662$ at $\beta=6.0$ and $b_m \approx -0.655$ at $\beta=6.15$. In the clover case, we have tried both these sets of $b_m$ values instead of our canonical procedure, but found only negligible changes in the central values, errors, and goodness of fits. For example, $f_B$ changes by less than 0.4% at $\beta=6.0$ and 0.1% at $\beta=6.15$. We do not, therefore, consider the standard improved quark mass further.

Since Eq. (12) is valid only through $\mathcal{O}(a)$, it is likely to produce large scaling errors if applied to the renormalization of the heavy-light axial vector current for heavy quarks with $am_{Q,0} \gtrsim 1$. Instead, the straightforward approach is to use the 1-loop, $\mathcal{O}(a)$, perturbative matching for clover fermions as calculated by Ishikawa, Onogi and Yamada [28,29]. We call this approach ''NP-IOY,'' where IOY refers to the authors, and NP indicates nonperturbative, because $c_{SW}$ has the value given in [7], and Eq. (12) is used in computing $f_\pi$.

Since Ref. [28] uses tadpole improvement defined through

[3] At $\beta=6.0$, Ref. [26] gets $b_A=1.28(3)(4)$, which is within our range. Note however, that Refs. [7,26] get quite different values of $c_A$ at $\beta=6.0$, indicating that effects of $\mathcal{O}(a^2)$ and higher play a significant role at this coupling.

$\kappa_c$ [29], just as we did above, we may summarize our application of their result as

$$A_0^{\text{NP-IOY}} = Z_A^{\text{IOY}} \overline{\tilde{q}_I} \gamma_0 \gamma_5 \tilde{Q}_I + Z_{12}^{\text{IOY}} \overline{\tilde{q}_I^0} \gamma_0 \gamma_5 a \vec{\gamma} \cdot \vec{D} \tilde{Q}_I^0, \quad (13)$$

where $\tilde{Q}_I$ and $\tilde{Q}_I^0$ are given by Eqs. (6) and (7) (and similarly for $\tilde{q}_I$ and $\tilde{q}_I^0$), and where

$$Z_A^{\text{IOY}} = 1 + \alpha_V(q^*) \rho_A^{(0)}$$

$$Z_{12}^{\text{IOY}} = -\alpha_V(q^*)(\rho_A^{(1)} + \rho_A^{(2)})/(2a\tilde{M}_2), \quad (14)$$

with $\rho_A^{(0)}$, $\rho_A^{(1)}$, and $\rho_A^{(2)}$ defined in [28]. We have used the fact that the operators $\overline{\tilde{q}_I} \gamma_0 \gamma_5 \vec{\gamma} \cdot \vec{D} \tilde{Q}_I$ and $-\overline{\tilde{q}_I} \vec{\gamma} \cdot \vec{D} \gamma_0 \gamma_5 \tilde{Q}_I$ have equal matrix elements between zero-momentum states, as is the case for our evaluation of decay constants, to combine the coefficients $\rho_A^{(1)}$ and $\rho_A^{(2)}$. For a central value of $q^*$, we take the result from the static-light calculation of Ref. [11], using the appropriate value of $c_{SW}$ and taking the heavy quark mass to be the mass of the $B$. This gives $q^* = 3.34/a$ at $\beta = 6.0$ and $q^* = 2.85/a$ at $\beta = 6.15$. Unlike [28], we include the $\tilde{d}_1$ factor for the light quark in the first term of Eq. (13). This is just for convenience, since $\tilde{d}_1$ is negligible for our light quarks. We have neglected $d_1$ for heavy and light quarks in the correction term (proportional to $Z_{12}^{\text{IOY}}$) in Eq. (13). We remark here that with our current data we use NP-IOY for $f_B$, $f_{B_s}$ but not for $f_D$, $f_{D_s}$ because the approximations in [28] are not applicable near the $D$ mass.

The errors in the NP-IOY calculation are formally $\mathcal{O}(a^2 \Lambda_{QCD}^2)$ and $\mathcal{O}(\alpha_V^2)$. Again, one should think of these errors as multiplied by an arbitrary $\mathcal{O}(1)$ function of $aM_Q$, making the $a$-dependence complicated in general. For example, if $M_Q$ is held fixed and $a$ is varied in the region where $aM_Q \sim 1$, linear $a$ dependence ($\sim a\Lambda_{QCD}^2/M_Q$) is possible.

Although NP-IOY is a well-defined approach to heavy-light physics with nonperturbative clover fermions, it does not take advantage for heavy quarks of the nonperturbative information in Eq. (12). An alternative, which has been used by the APE [30] and UKQCD [16] Collaborations, is to apply Eq. (12) for moderate $am_{Q,0}$, where it is still approximately justified, and then extrapolate up to the $B$ mass. That approach has two main systematic errors: First, one has no guidance from heavy quark effective theory (HQET) about the order of the polynomial in $1/m_Q$ with which to extrapolate to the $B$ mass, and second $\mathcal{O}(a^2)$ errors, while relatively small for the moderate masses studied, can grow rather larger when extrapolated over a wide mass range. We prefer instead a different method, which we call "NP-tad" for reasons discussed below. The idea here is to replace Eq. (12) by an equivalent expression through $\mathcal{O}(a)$ but which has the advantage of having a reasonable limit for large $am_{Q,0}$. The modified Eq. (12) is then used directly at or near the $B$ mass.

Equation (12) applied to a heavy-light current gives

$$A_0^{\text{NP}} = Z_A^{\text{NP}} \sqrt{4\kappa_Q \kappa_q} \left(1 + b_A \frac{am_{Q,0} + am_{q,0}}{2}\right) \times [A_0 + c_A a \partial_0 P_5],$$

$$A_0 = \overline{q} \gamma_0 \gamma_5 Q; \quad P_5 = \overline{q} \gamma_5 Q. \quad (15)$$

Note that $A_0^{\text{NP}}$ does not approach a static limit for $am_{Q,0} \to \infty$. Instead, it goes to $-\infty$ because $c_A < 0$ and $\partial_0 P_5 \sim \sinh(M_{Qq,1}) \sim am_{Q,0}$. ($M_{Qq,1}$ is the meson pole mass.) Even if $c_A$ were zero, $A_0^{\text{NP}}$ would still blow up because of the term $b_A am_{Q,0}$. For this reason, small discretization errors for moderate $am_{Q,0}$ may be magnified significantly if Eq. (15) is used to extrapolate to the $B$.

To define the NP-tad alternative, we first let

$$R(M_{Qq}) \equiv \frac{\langle 0 | \partial_0 P_5 | Qq \rangle}{(m_{Q,0} + m_{q,0}) \langle 0 | A_0 | Qq \rangle}, \quad (16)$$

where $Qq$ is a generic heavy-light pseudoscalar meson. Due to a cancellation of $\sinh(M_{Qq,1})$ (from $\partial_0$) and the explicit $m_{Q,0}$ in the denominator, one expects $R$ has a finite limit as $am_{Q,0} \to \infty$. This is confirmed by our simulations. Then

$$A_0^{\text{NP}'} = Z_A^{\text{NP}} \sqrt{4\kappa_q \kappa_Q} \sqrt{1 + (b_A + 2c_A R) am_{Q,0}} \times \sqrt{1 + (b_A + 2c_A R) am_{q,0}} A_0 \quad (17)$$

gives results for $\langle 0 | A_0^{\text{NP}'} | Qq \rangle$ that are identical to $\langle 0 | A_0^{\text{NP}} | Qq \rangle$ through $\mathcal{O}(a)$. However, because $\kappa_Q am_{Q,0} \to 1/2$ as $\kappa_Q \to 0$, Eq. (17) has a static limit, unlike Eq. (12).

The mass dependence of Eq. (17) is in fact very similar to the Fermilab formalism at tadpole-improved tree level. Indeed, from Eqs. (6) and (5), the Fermilab version of Eq. (17) is

$$A_0^{\text{FNAL}} = Z_A \sqrt{4\kappa_q \kappa_Q} \sqrt{1 + am_{Q,0}/u_0} \times \sqrt{1 + am_{q,0}/u_0} A_0, \quad (18)$$

where $Z_A = Z_A^{tad} u_0$ is the renormalization constant for the axial vector current without the tadpole factor removed, and where we have dropped the $d_1$ terms for simplicity. Hence Eq. (17) is equivalent to Eq. (18) but with a special (mass-dependent) value for the tadpole factor: $u_0 = (b_A + 2c_A R)^{-1}$. The similarity to tadpole improvement (within the context of nonperturbative renormalization) is the reason for the name "NP-tad." Note that, at tree level, where $b_A = Z_A = u_0 = 1$ and $c_A = 0$, NP-tad is in fact identical to the Fermilab approach.

In practice, we put the $d_1$ terms as well as the corresponding perturbative subtraction back into the axial vector current. Thus Eq. (17) becomes

$$A_0^{\text{NP - tad}} = Z_A^{\text{NP}} \sqrt{4\kappa_q \kappa_Q} \sqrt{1 + (b_A + 2c_A R) am_{Q,0}} \times \sqrt{1 + (b_A + 2c_A R) am_{q,0}} A_0^{\text{d1 - sub}} \quad (19)$$

with

TABLE I. Lattice parameters. The upper group corresponds to quenched lattices; the lower group, to dynamical lattices with $N_f=2$ staggered quarks. The set G was generated by HEMCGC [35]. Sets marked by * are new since Ref. [4]. Heavy and light Wilson quark propagators were generated on all sets except J and 5.7-large. On the latter set, which includes lattices of various sizes, only light quark propagators were generated. Normal (''thin-link'') clover propagators were computed on set J and CP1, a 199 lattice subset of CP. (See Table II for thin-link clover parameters.) Fat-link clover propagators were generated on set CPF (a 99 configuration subset of CP1) and RF (a 98 configuration subset of set R).

| Name | $\beta$ ($am_q$) | Size | No. confs. |
|---|---|---|---|
| A | 5.7 | $8^3\times 48$ | 200 |
| B | 5.7 | $16^3\times 48$ | 100 |
| 5.7-large | 5.7 | $12^3\times 48$, $16^3\times 48$, $20^3\times 48$, $24^3\times 48$ | 403, 390, 200, 184 |
| E | 5.85 | $12^3\times 48$ | 100 |
| C | 6.0 | $16^3\times 48$ | 100 |
| *CP | 6.0 | $16^3\times 48$ | 305 |
| *J | 6.15 | $20^3\times 64$ | 100 |
| D | 6.3 | $24^3\times 80$ | 100 |
| H | 6.52 | $32^3\times 100$ | 60 |
| L | 5.445 (0.025) | $16^3\times 48$ | 100 |
| N | 5.5 (0.1) | $24^3\times 64$ | 100 |
| O | 5.5 (0.05) | $24^3\times 64$ | 100 |
| M | 5.5 (0.025) | $20^3\times 64$ | 199 |
| P | 5.5 (0.0125) | $20^3\times 64$ | 199 |
| *U | 5.6 (0.08) | $24^3\times 64$ | 202 |
| *T | 5.6 (0.04) | $24^3\times 64$ | 201 |
| *S | 5.6 (0.02) | $24^3\times 64$ | 202 |
| G | 5.6 (0.01) | $16^3\times 32$ | 200 |
| R | 5.6 (0.01) | $24^3\times 64$ | 200 |

$$A_0^{\text{d1 - sub}} \equiv [1+\alpha_V(q^*)\rho_A^{(\text{sub})}]A_0 + \bar{q}\gamma_0\gamma_5 a\tilde{d}_1\vec{\gamma}\cdot\vec{D}Q - \bar{q}a\tilde{d}_1\vec{\gamma}\cdot\vec{D}\gamma_0\gamma_5 Q, \quad (20)$$

where $\rho_A^{(\text{sub})}$ is the IOY perturbative correction coming from the $d_1$ terms alone, which we extract by comparing the complete perturbative result computed with and without the terms [31]. In Eq. (20), $\tilde{d}_1=d_1(a\tilde{m}_{Q,0})$ and $\tilde{d}_1=d_1(a\tilde{m}_{q,0})$ in the second and third terms, respectively, with $d_1(am_0)$ given in Eq. (4). As before, $d_1(a\tilde{m}_{q,0})$ is negligible and is included merely for convenience.

Equations (19) and (20) define the NP-tad approach. The errors of NP-tad are formally $\mathcal{O}(a^2\Lambda_{QCD}^2)$ and $\mathcal{O}(a^2M_Q^2)$. Thus, the errors could in principle be large as $M_Q$ increases at fixed $a$. The hope is that the requirement that the decay constants have a limit as $M_q\to\infty$ has forced the $a^2M_Q^2$ (and higher) terms to have small coefficients, but this is not proven. We emphasize that the NP-tad approach is logically neither better nor worse than the method of Refs. [16,30] for $B$ physics. NP-tad is an attempt to keep the nonperturbative $\mathcal{O}(a)$ information and yet include some higher effects in a smooth way, but there is no *a priori* guarantee that all or most of such effects are included. *A posteriori*, one can compare how well the methods scale with lattice spacing. The scaling of NP-tad results currently appears to be comparable to that seen with standard nonperturbative normalization and extrapolation in Ref. [16].[4] With only two lattice spacings in the NP-tad data and in [16], however, this comparison is far from definitive. We therefore use the NP-IOY approach (whose errors are better understood), in addition to both the NP-tad method and standard Wilson fermions, in determining the central value and errors.

## III. COMPUTATIONAL DETAILS

### A. Lattice generation and inversion

Table I shows the lattice parameters used. Quenched lattices are generated using a standard combination of pseudoheat bath [32] and overrelaxed [33] updates. Successive configurations are separated by 200 iterations, where each iteration consists of 1 heat bath and 4 (9 for set H, $\beta=6.52$) overrelaxed sweeps. The sets J and CP are new additions to the quenched lattices previously analyzed in Ref. [4]. Dynamical fermion lattices were separated by 10 trajectories (each of unit molecular dynamics time) of the R algorithm [34]. (Set G, from HEMCGC [35], is separated by 10 trajectories of time $1/\sqrt{2}$ in MILC units.)

[4]An earlier version of Ref. [16] showed considerably worse scaling, but that appears to have been associated more with the use of scale $r_0$ from the potential than with the normalization and extrapolation.

Unimproved Wilson valence fermion propagators were generated for all these sets except J. (On set 5.7-large only light Wilson propagators were computed.) Because our calculations were initially limited by slow I/O speeds and lack of long-term storage, we performed the calculations of heavy-light meson propagators ''on the fly''—i.e., without storing quark propagators. The hopping parameter expansion of the heavy quark propagator, as proposed by Henty and Kenway [36], makes this possible. Further, the expansion allows us to study a large number of heavy quark masses, with almost no additional expense. For this reason, we continued using the approach of Ref. [36] even after faster I/O and better storage became available.

In the hopping-parameter approach, the light quark propagator, for a single spin-color source, is first computed with standard methods (red-black preconditioning; minimal residual). The heavy quark propagator for the same spin-color source is then computed order by order in the heavy hopping parameter. At each order, the contribution to the meson propagators, summed over space, is stored to disk. The full meson propagator for any heavy hopping parameter, $\kappa_Q$, can then be reconstructed after the fact by multiplying the stored results by appropriate powers of $\kappa_Q$ and summing over iterations as well as spin and color. Propagators in the static-light limit, where the heavy quark mass is taken to infinity, can be obtained as a by-product of this procedure.

Our quark sources are Coulomb-gauge Gaussians. We run the overrelaxed gauge fixer until the sum of the trace of all spacelike links (normalized to 1 when all links are unit matrices) changes by less than $7\times10^{-7}$ per pass. This takes, for example, about 435 passes on set D, and a comparable number of passes on the other sets.

Our Wilson light quark propagators are computed for three values of $\kappa_q$, giving light quark masses ($m_q$) in the range $0.7m_s \lesssim m_q \lesssim 2.0m_s$, where $m_s$ is the strange quark mass. We analyze heavy-light mesons with 8 to 10 heavy quark masses per data set, with heavy-light pseudoscalar meson masses ($M_{Qq}$) in the range $1.25\ \mathrm{GeV} \lesssim M_{Qq} \lesssim 4.0$ GeV. The heavy quark propagators are computed with 400 passes of the hopping parameter expansion. Figure 1 shows the convergence on set D of the hopping parameter expansion for heavy-light meson correlators at the maximum time separation (half-way across the lattice). The value of $\kappa_Q$ (0.1456) used in Fig. 1 gives a meson mass of $M_{Qq} \sim 1.1$ GeV when the light quark $\kappa_q$ is extrapolated to $\kappa_{u,d}$. Since 1.1 GeV is slightly lighter than the lightest value used in our analysis, we are confident that the expansion is under control.

Because the heavy-light mesons must be constructed at each of the 400 orders of the hopping parameter expansion, it is too expensive to sum the central point of the smeared sinks over the entire spatial volume, even using fast Fourier transforms (FFT's). Instead, we simply sum over 16 points in the $L^3$ spatial volume: the 8 points (0,0,0), ($L$/2,0,0), (0,$L$/2,0), . . . , ($L$/2,$L$/2,0), . . . , plus the 8 points obtained by adding ($L$/4,$L$/4,$L$/4) to each of the previous points. This fixes the lowest nonzero momentum which contributes to be (2,2,0) (and permutations) in units of $2\pi/L$. For the heavy-light mesons studied here, these higher momentum states are suppressed sufficiently at asymptotic Euclidean time by their higher energy. However, in the largest physical volumes, sets N, O, U, and T, the higher momentum states for the heaviest mesons are quite close to the ground state, and we are required to go to large times ($t_{\min}/a \sim 22$–$27$) for the smeared-smeared propagators in order to make single exponential fits with good confidence levels.

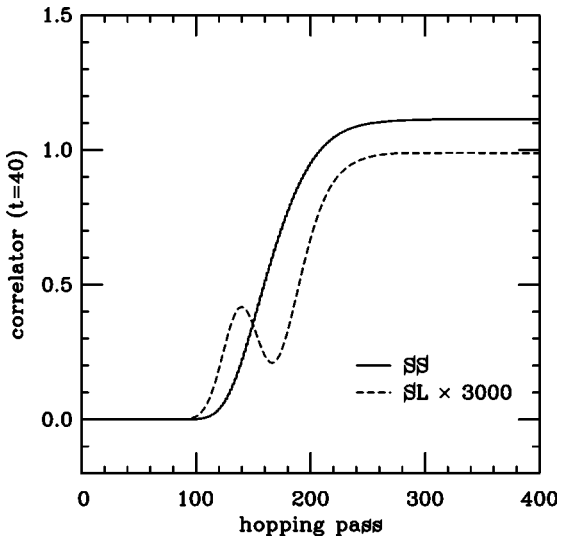


FIG. 1. Convergence of the hopping parameter expansion for heavy-light pseudoscalar meson correlators on set D. $\kappa_Q = 0.1456$, while $\kappa_q = 0.1507$, the lightest of the three light quarks analyzed on this set. The values of the smeared-smeared and smeared-local correlators at $t = 40$ (half-way across the lattice) are shown with the solid and dashed lines, respectively.

The static-light mesons have no such suppression, and the contribution of higher momentum states is limited only by their overlap with the sources. Using computed static-light wave functions [37], we find that the contamination in static-light decay constants from nonzero momentum states is small ($\approx 0.7\%$) for lattices with spatial size of $\approx 1.5$ fm (sets A, C, CP, D, E, G, H). However, on all other (larger) sets the contamination is expected to be large. We therefore have performed a dedicated static-light computation on those lattices, with relative smearing functions taken from [38] and zero momentum intermediate states enforced by a complete FFT sum over spatial slices. In addition, the dedicated static light computation has been run on sets A and E (because the plateaus from the hopping method proved to be poor) and sets G and CP (as a check of the hopping method). On the latter sets, the two methods give consistent results, but we choose the dedicated method because the errors are smaller. Thus, only on sets C, D, and H is the hopping approach used for the final analysis of the static-light mesons.

Standard (''thin-link'') clover improved valence quark propagators have been generated using stabilized biconjugate gradient inversion [39] (for light quarks) and the hopping parameter expansion (for heavy quarks) on quenched sets J and ''CP1,'' a 199-lattice subset of CP. In this case we have 5 light and 5 heavy quark masses, in the same range as for the Wilson valence quarks. For the heavy quarks we sum, on the fly, the orders in the hopping expan-

TABLE II. Parameters used for nonperturbative, thin-link clover fermions (quenched configurations).

| Set | $\beta$ | No. confs. | $c_{SW}$ | $Z_A$ | $c_A$ | $b_A$ | $b_A$ range |
|---|---|---|---|---|---|---|---|
| CP1 | 6.0 | 199 | 1.769 | 0.7924 | −0.0828 | 1.472 | 1.256→1.586 |
| J | 6.15 | 100 | 1.644 | 0.8050 | −0.0426 | 1.423 | 1.244→1.510 |

sion for a given $\kappa_Q$—i.e., this is a standard inversion, which does not allow a choice of arbitrary $\kappa_Q$ after the fact. However, our experience with the Wilson case leads us to believe that a large number of heavy quark masses is unnecessary: the behavior of $f_{Qq}\sqrt{M_{Qq}}$ with $1/M_{Qq}$ is quite smooth. Further, we are now able to perform an FFT sum of the meson propagators, so that zero momentum is enforced and contamination from excited states is reduced. The full Fermilab formalism allows us to choose heavy quark masses near the *b* quark mass in this case; we therefore do not need to compute static-light mesons here to stabilize an extrapolation.

As explained in Sec. II B, we take the ALPHA Collaboration [7] values, where available, for the normalization and improvement constants of our clover fermions. The parameters used are shown in Table II.

### B. Covariant fits

We need to fit correlators in time, extrapolate/interpolate in light and heavy quark masses, and extrapolate in lattice spacing to the continuum. In all cases except the last, the data are correlated, so covariant fits are preferable. As is well known [40], however, it requires a large statistical sample to determine accurately the small eigenvalues of the covariance matrix. With limited statistics, such eigenvalues will be poorly determined and can make the covariant fits unstable. This is a particular problem in the current analysis because the large time dimension of our lattices and the fact that we fit two channels simultaneously means that we often make fits with 25 or more degrees of freedom.

The technique we use to deal with the problem of small eigenvalues has many similarities to the methods proposed in [40] but has some advantages in our analysis. It is based on a standard approach in factor analysis [41]. We first compute the correlation matrix (the covariance matrix, but normalized by the standard deviations to have 1's along the diagonal) and find its eigenvalues and eigenvectors. We then reconstruct the correlation matrix from the eigenvectors, but omitting those corresponding to eigenvalues less than $\lambda_{\rm cut}$, a cutoff. The resulting matrix is of course singular. It is made into an acceptable correlation matrix by restoring the 1's along the diagonal. Finally, the corresponding covariance matrix is constructed (by putting back the standard deviations), inverted, and used in the standard way for making the fits.

The above technique interpolates smoothly between standard covariant fits, where no eigenvalues are omitted, and noncovariant (uncorrelated) fits, where all eigenvalues are omitted. Furthermore, because the correlation (as opposed to covariance) matrix is used, the eigenvalues are normalized, with the average eigenvalue always equal to 1. This allows us to make a uniform determination of which eigenvalues to keep, which is very important since we are dealing with thousands of fits, and it is impossible to examine each fit by hand. Our standard procedure is to choose $\lambda_{\rm cut}=1$, i.e., we drop all eigenvalues less than 1. The eigenvectors kept typically account for 90–95 % of the total covariance. Indeed, when one changes how the covariance matrix is computed (for example, by increasing the number of configurations eliminated in the jackknife), the eigenvalues smaller than 1 generally change drastically with our typical sample size of $\sim$100. The approach eliminates unstable, ''pathological'' fits completely.

We have checked that the final results are not significantly affected when we keep several more (or several fewer) eigenvalues throughout. Furthermore, on our set with the greatest statistics (set CP, 305 configurations) we are able to compare with a wide variety of different cuts on the eigenvalue, as well as standard covariant fits where all eigenvalues are kept. We find that central values almost always agree within one statistical sigma, and usually differ by much less than that. In data discussed below (and tabulated at http://www.physics.wustl.edu/~cb/Nf=2_tables) we show for comparison fits with different eigenvalue cuts for this set.

One disadvantage of the current approach, as well as to the methods in [40], is that there is no true quantitative measure of ''goodness of fit.'' When eigenvalues are removed, the truncated chi-squared, $\chi^2_{\rm cut}$, tends to be (but is not always) considerably smaller than the ''true'' $\chi^2$ from a complete covariant fit. However, our experience has shown that requiring $\chi^2_{\rm cut}/{\rm d.o.f.}<1$ with $\lambda_{\rm cut}=1$ produces fits that are almost always acceptable by a standard criterion (C.L. $>0.05$, with C.L. the confidence level) when the data allow a fully covariant (uncut) fit. This is not the case for noncovariant fits ($\lambda_{\rm cut}=\infty$). Such fits may have $\chi^2_{\rm cut}/{\rm d.o.f.}\ll 1$ and yet extend to a fully covariant fit with extremely small C.L. For example, exponential fits to a correlator which include several points clearly outside the plateau region can still have $\chi^2_{\rm cut}/{\rm d.o.f.}\ll 1$ when $\lambda_{\rm cut}=\infty$, but not, in our experience, when $\lambda_{\rm cut}=1$.

At every stage in the analysis, we compute statistical errors by the jackknife procedure. The covariance matrices are also computed by jackknife. For the quenched sets, there is no evidence of a nonzero autocorrelation length. However, in the dynamical sets, the errors typically increase with the number of configurations omitted in the jackknife until $\sim$4 configurations are omitted. To be conservative, we determine our statistical errors and covariance matrices by omitting 8 configurations at a time (for both dynamical and quenched sets).

### C. Correlator fits and extraction of decay constants

We compute ''smeared-local'' and ''smeared-smeared'' pseudoscalar meson propagators in each of three cases:

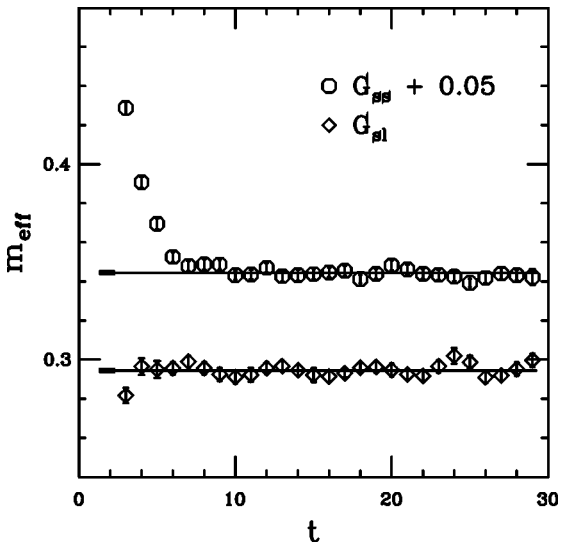


FIG. 2. Light-light effective masses for set R, $\kappa=0.159$. The fit ranges are 8 to 31 for $G_{SL}$ and 10 to 31 for $G_{SS}$. The smeared-smeared masses are shifted upward for clarity. The long horizontal lines show the fit value of the mass. The error in the fit value is indicated at the left end of the fit lines by two short horizontal lines.

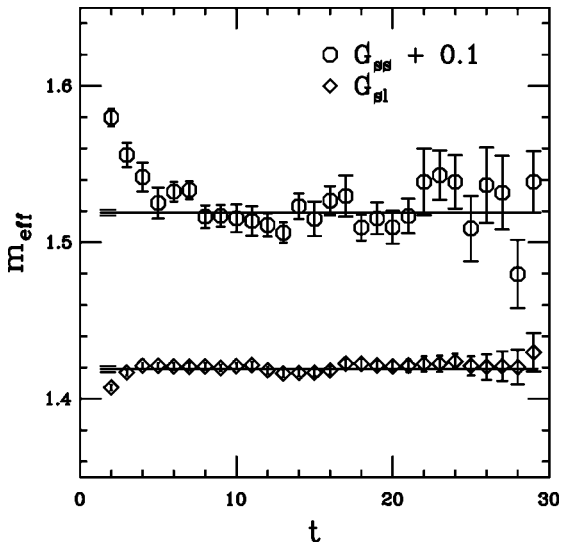


FIG. 3. Same as Fig. 2, but for heavy-light effective masses on set J, $\kappa_Q=0.098$, $\kappa_q=0.1347$. The fit ranges are 12 to 18 for $G_{SL}$ and 8 to 16 for $G_{SS}$.

heavy-light, static-light, and light-light (the last with degenerate masses only). These correlators are defined by

$$G_{SL}(t)=\sum_{\vec{x}} \langle 0|A_0^R(\vec{x},t)\chi_5^\dagger(\vec{0},0)|0\rangle \tag{21}$$

$$G_{SS}(t)=\sum_{\vec{x}}{}' \langle 0|\chi_5(\vec{x},t)\chi_5^\dagger(\vec{0},0)|0\rangle, \tag{22}$$

where $A_0^R$ is the relevant renormalized current, namely $A_0^{\rm KUR}$ [Eq. (10)], $A_0^{\rm STAT}$ [Eq. (11)], $A_0^{\rm NP\text{ - }IOY}$ [Eq. (13)], $A_0^{\rm NP\text{ - }tad}$ [Eq. (19)], or $A_0^{\rm NP}$ [Eq. (12)—for light-light quantities only]. For $G_{SS}$, the prime on the sum indicates that only $N_{\rm sink}$ points on a time-slice are included. As discussed above, for all the Wilson heavy-light and light-light data, $N_{\rm sink}=16$. For the clover and the dedicated static computations, the complete sum is performed (with FFT), so one has $N_{\rm sink}=V\equiv n_x n_y n_z$. In Eqs. (21) and (22), $\chi_5$ is the Gaussian pseudoscalar source, given by

$$\chi_5(\vec{x},t)=\sum_{\vec{y}\vec{z}} e^{-\vec{y}^2/r_0^2}e^{-\vec{z}^2/r_0^2}\overline{q}(\vec{x}+\vec{y})\gamma_5 Q(\vec{x}+\vec{z}). \tag{23}$$

The width $r_0$ varies from 2.33 lattice spacings (set A) to 8 spacings (set H) and is chosen to be roughly 0.35 fm. For the Henty-Kenway hopping calculations, the sums in Eq. (23) run over even $\vec{y}$, $\vec{z}$ only, so that we may exploit an even-odd decomposition. In Eq. (23) and below, we use the notation of the heavy-light case (quarks $Q$ and $q$) generically: for light-light formulas, let $Q\to q$; for static-light formulas, let $Q\to h$.

For large Euclidean time $t$, $G_{SL}$ and $G_{SS}$ are fit simultaneously and covariantly to single exponential forms, with the same mass in both channels

$$G_{SL}\to\zeta_{SL}e^{-Mt};\quad G_{SS}\to\zeta_{SS}e^{-Mt}. \tag{24}$$

In other words, these are fits with three parameters: $M$, $\zeta_{SL}$ and $\zeta_{SS}$. Central values use $\lambda_{\rm cut}=1.0$ throughout, except for set CP, where $\lambda_{\rm cut}=0.1$. Typical effective mass plots for the light-light and heavy-light cases are shown in Figs. 2, 3, and 4, respectively. Here and below, we generally choose $N_f=2$ and clover data for the plots because the quenched Wilson data have been discussed in more detail previously [4,5].

We vary the fit range (in $t$) in each channel over several choices that appear to be in the asymptotic, ''plateau,'' region

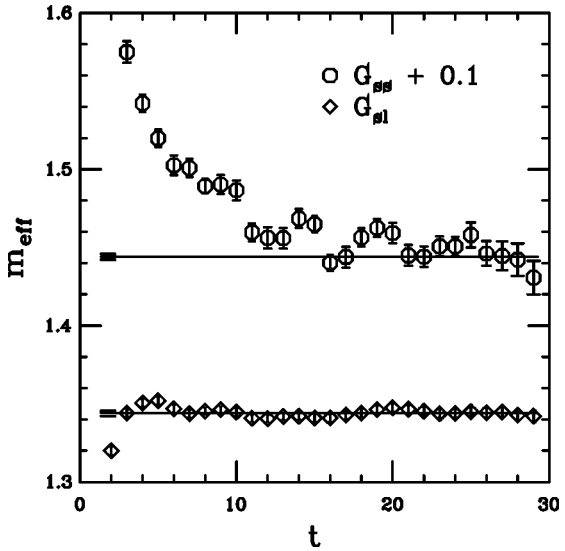


FIG. 4. Same as Fig. 2, but for heavy-light effective masses for set M, $\kappa_Q=0.120$, $\kappa_q=0.160$. Fit ranges are 13 to 31 for $G_{SL}$ and 19 to 31 for $G_{SS}$. The heavy quark is computed with the Henty-Kenway hopping expansion. The late plateau in $G_{SS}$ is due to contamination from nonzero momentum states because the sink is not summed over complete time slices.

for the effective mass. Combining such choices for the light-light, heavy-light and static-light cases, we have approximately 25 different versions of the analysis on each data set. Our central values are taken from the version which has the best blend of small statistical errors and low, or at least acceptable, values of $\chi^2_{\rm cut}$/d.o.f. Here "acceptable" is defined, with few exceptions, as $\chi^2_{\rm cut}$/d.o.f.$<1.3$, with $\lambda_{\rm cut}=1$. (In about 85% of the central value choices, $\chi^2_{\rm cut}$/d.o.f.$<1$.) The exceptions are (i) a few fits to heavy-light mesons outside the ranges of mass that we include in our final determinations of the decay constants, (ii) a few fits to heavy-light mesons on the largest lattices, where the slow approach to the asymptotic regime for smeared-smeared correlators computed with the Henty-Kenway approach (see Sec. III A) left us with somewhat noisy data at large $t$, and (iii) the fit to the static-light meson with heaviest light quark on set G, which had rather noisy data. In these exceptional cases, we relax our definition of acceptable $\chi^2_{\rm cut}$/d.o.f. to be less than 1.9, 1.7, and 1.6, respectively.

Of course, with the approximately 900 channels we fit, one should expect that some fits over truly asymptotic ranges will have poor $\chi^2$/d.o.f. simply because of statistical fluctuations. However, since our $\chi^2_{\rm cut}$ generally underestimates the full $\chi^2$, we have tried to make choices which are more conservative than a standard criterion, of say, confidence level $>0.05$.

From the fits, the pseudoscalar decay constants $f_{Qq}$ for given quark masses are then obtained via

$$f_{Qq}\sqrt{M_{Qq}}=\frac{\sqrt{2}}{a^{3/2}}\sqrt{\frac{N_{\rm sink}}{V}}\frac{\zeta_{SL}}{\sqrt{\zeta_{SS}}}, \tag{25}$$

where we use the definition of the decay constant that gives $f_\pi=130.7$ MeV:

$$\langle 0|A_0^{\rm cont}|Qq,\vec{p}=0\rangle\equiv -if_{Qq}M_{Qq}, \tag{26}$$

with $A^{\rm cont}$ the continuum axial vector current.[5]

Data for the masses and decay constants for each of the sets listed in Table I are posted at http://www.physics.wustl.edu/~cb/Nf=2_tables. The files "*name*_qq.dat," where "*name*" is the set name (A, B, E, . . . ) give dimensionless light-light masses and decay constants as a function of hopping parameter. Similarly "*name*_Qq.dat" and "*name*_Statq.dat" give dimensionless masses and values for $a^{3/2}f_{Qq}\sqrt{M_{Qq}}$ for heavy-light and static-light mesons, respectively. For set CP, additional files, with "lambda-cut=X" appended to the name, show the effect of various truncations of the correlation matrix. For heavy-light mesons the masses tabulated are the shifted masses $aM_{Qq,2}$, Eq. (8); for the static-light case they are simply the pole masses. Time ranges, number of degrees of freedom, and $\chi^2_{\rm cut}$ are included for all fits. For sets CP1 and J, the nonperturbative clover lattices, "*name*" gets a further qualifier in the heavy-light case, which is either "NP-IOY" or "NP-tad" for the two types of renormalization performed.

To enable the reader to see the effects of various renormalizations used, as well as to make possible reanalysis of the data by other groups, we have tabulated additional raw data. For all sets, we have separately computed correlators of the bare lattice axial current $A_0$:

$$G_{SL}^{bare}(t)=\sum_{\vec{x}}\langle 0|A_0(\vec{x},t)\chi_5^\dagger(\vec{0},0)|0\rangle;\quad A_0=\overline{q}\gamma_0\gamma_5 Q. \tag{27}$$

We fit $G_{SL}^{bare}$ simultaneously with $G_{SS}$, as in Eq. (24), giving us the three quantities $M$, $\zeta_{SL}^{\rm bare}$ and $\zeta_{SS}$. We then define $\Xi^{\rm bare}$ by

$$\Xi^{\rm bare}=\sqrt{\frac{N_{\rm sink}}{V}}\frac{\zeta_{SL}^{\rm bare}}{\sqrt{\zeta_{SS}}}. \tag{28}$$

$\Xi^{\rm bare}$ is basically the unrenormalized decay constant. For example, in the case of our heavy-light Wilson data, for which the renormalized current is given by Eq. (10), we have

$$f_{Qq}\sqrt{M_{Qq}}=\frac{\sqrt{2}}{a^{3/2}}Z_A^{\rm KUR}\sqrt{1-\frac{3\kappa_Q}{4\kappa_c}}\sqrt{1-\frac{3\kappa_q}{4\kappa_c}}\Xi^{\rm bare}. \tag{29}$$

The masses and quantities $\Xi^{\rm bare}$ are posted in the files "*name*_qq_bare.dat," "*name*_Qq_bare.dat," "*name*_Statq_bare.dat."[6]

For heavy-light mesons with the nonperturbative clover action, we have posted additional intermediate data. We define

$$A_0^{\rm dim4}\equiv\overline{q}\gamma_0\gamma_5 a\vec{\gamma}\cdot\vec{D}Q \tag{30}$$

$$A_0^{d_1}\equiv A_0+[d_1(a\tilde{m}_{Q,0})+d_1(a\tilde{m}_{q,0})]A_0^{\rm dim4} \tag{31}$$

$$A_0^{d_1-{\rm sub}}=[1+\alpha_V(q^*)\rho_A^{\rm (sub)}]A_0 +[d_1(a\tilde{m}_{Q,0})+d_1(a\tilde{m}_{q,0})]A_0^{\rm dim4} \tag{32}$$

$$A_0^{\rm imp}\equiv\sqrt{1+(b_A+2c_AR)am_{Q,0}}\times\sqrt{1+(b_A+2c_AR)am_{q,0}}A_0^{d_1-{\rm sub}}, \tag{33}$$

where "imp" stands for "improved," and where Eq. (32) is a rewriting of Eq. (20), using the fact that the operators

[5]When Eq. (25) is used for static-light mesons with the Henty-Kenway hopping approach, an extra factor of $\sqrt{2}$ is required on the right-hand side. This arises from the fact that the highest momentum state $(\pi,\pi,\pi)$ aliases the zero momentum state with our even-site-only source, and the higher momenta are not suppressed in Euclidean time for the static case.

[6]Again, for static-light correlators computed with the hopping approach, we include an extra factor of $\sqrt{2}$ on the right-hand side of Eq. (28). In this case the heavy-light masses tabulated are the (pole) masses directly from the fits, not the shifted masses.

$\bar{\tilde{q}}_I \gamma_0 \gamma_5 \vec{\gamma}\cdot\vec{D}\tilde{Q}_I$ and $-\bar{\tilde{q}}_I \vec{\gamma}\cdot\vec{D}\gamma_0\gamma_5\tilde{Q}_I$ have equal zero-momentum matrix elements. For each current in Eqs. (30)–(33), we define a corresponding $\Xi$, as in Eq. (28). Results for $\Xi^{\mathrm{dim4}}$, $\Xi^{d_1}$, $\Xi^{d_1\text{-sub}}$, and $\Xi^{\mathrm{imp}}$ are tabulated in the files "*name*_Qq_intermediate.dat," where "*name*" now is just CP1 or J. From Eqs. (13), (6), (30), and (31), these quantities are related to the decay constants in the NP-IOY case by

$$f_{Qq}\sqrt{M_{Qq}} = \frac{\sqrt{2}}{a^{3/2}}\sqrt{1-\frac{3\kappa_Q}{4\kappa_c}}\sqrt{1-\frac{3\kappa_q}{4\kappa_c}} \times [Z_A^{\mathrm{IOY}}\Xi^{d_1} + Z_{12}^{\mathrm{IOY}}\Xi^{\mathrm{dim4}}]. \quad (34)$$

Similarly, from Eqs. (19), (32), and (33), we have in the NP-tad case:

$$f_{Qq}\sqrt{M_{Qq}} = \frac{\sqrt{2}}{a^{3/2}} Z_A^{\mathrm{NP}}\sqrt{4\kappa_Q\kappa_q}\,\Xi^{\mathrm{imp}} \quad (35)$$

$$= \frac{\sqrt{2}}{a^{3/2}} Z_A^{\mathrm{NP}}\sqrt{4\kappa_Q\kappa_q}\sqrt{1+(b_A+2c_AR)am_{Q,0}} \times \sqrt{1+(b_A+2c_AR)am_{q,0}}\,\Xi^{d_1-\mathrm{sub}}. \quad (36)$$

In practice, when Eqs. (24) and (25) are used to compute $f_{Qq}\sqrt{M_{Qq}}$, Eqs. (34) and (36) are obeyed only up to small corrections. This is because two separate fits are performed to compute the two terms in Eq. (34); whereas the quantities are added first and then fit in Eq. (24). For Eq. (36), the discrepancy is due to the fact that the factors like $\sqrt{1+(b_A+2c_AR)am_{Q,0}}$ and their errors are not included in the fit here, but are factored in later.

Finally, we also compute smeared-local light-light vector meson propagators. These are fit covariantly to single exponentials (two parameter fits). Raw data for the vector channel appear in the files "*name*_qq-vector.dat."

### D. Chiral extrapolations

Chiral extrapolations/interpolations are needed for the light-light pseudoscalars, which are used to set the scale (through $f_\pi$) and to find $\kappa_c$ and the physical values of $\kappa_{u,d}$ and $\kappa_s$, the hopping parameters of the up/down and strange quarks. (We generally determine $\kappa_s$ by adjusting the degenerate pseudoscalar mass to $\sqrt{2m_K^2-m_\pi^2}$, the tree-level chiral perturbation theory value.) The light-light vectors provide alternative determinations of the scale (through $m_\rho$) and $\kappa_s$ (through $m_\phi$) and require additional chiral extrapolations. The heavy-light and static-light masses and decay constants also need to be extrapolated/interpolated in light quark mass to the up/down and strange quark masses.

We have tried chiral extrapolations using either the bare light quark mass $m_{q,0}$ or the light quark tadpole-improved kinetic mass $\tilde{M}_{q,2}$ as the independent variable.[7] For both Wilson and clover quarks, the confidence level of linear fits to $M_{Qq}$, $f_{Qq}$, and $f_{qq}$ is better with $\tilde{M}_{q,2}$ than $m_{q,0}$, so we use it from now on in all cases.

An important question is which functional form one should fit to. Unfortunately, as in other lattice computations to date, we have been forced to work at fairly large values of light quark mass. In this region, our data for decay constants, both $f_{Qq}$, and $f_{qq}$, are quite linear. There is little evidence for chiral logarithms, which should introduce significant curvature as one approaches the chiral limit, as emphasized recently by Kronfeld and Ryan [8] and Yamada [9]. This is presumably not a problem with chiral perturbation theory ($\chi$PT), but simply an indication that higher order terms (e.g., terms quadratic in quark mass) are as important as the chiral log terms in the current mass regime. Further, chiral log fits would introduce yet another parameter in the heavy-light case, the $B$-$B^*$-$\pi$ coupling $g$.[8] It therefore seems clear to us that fits of $f_{Qq}$ to the NLO $\chi$PT form would require at least four parameters: the value in the chiral limit, a linear slope, the coefficient $g^2$, and a higher order (quadratic?) term introduced to cancel most of the curvature of the logarithms in our relatively high mass region. With only three light quark masses on most sets, it is clear that such an approach is not feasible at present. In work in progress [45], however, we are consistently using five light quark masses and expect that we will be able to include chiral logs and quadratic terms directly in the fits for central values.

For our "standard" chiral extrapolations, we thus consider only quadratic and linear fits in $\tilde{M}_{q,2}$. For each physical quantity, we choose one of these fits for the central value, and the other is taken, where appropriate, to give a standard chiral extrapolation error. Note that $f_B$ [46] and $f_\pi$ [47] have similar chiral log effects in full QCD:

$$f_B = f_B^0\left[1+\frac{1}{16\pi^2 f^2}\left(-\frac{3(1+3g^2)}{4}m_\pi^2\ln(m_\pi^2)+\cdots\right)\right] \quad (37)$$

$$f_\pi = f\left[1+\frac{1}{16\pi^2 f^2}[-2m_\pi^2\ln(m_\pi^2)+\cdots]\right]. \quad (38)$$

Since we fix the lattice scale with $f_\pi$ and always use the same type of chiral fit for both $f_{Qq}$ and $f_{qq}$, it is not unreasonable to expect that much of the systematic effect coming from not including the curvature of Eqs. (37) and (38) will cancel. In Secs. III E and V D, we explain how we test this assumption and estimate the chiral logarithm effects in the dynamical case.

[7] As discussed in Sec. II B, we also tried the standard $\mathcal{O}(a)$ improved quark mass in the clover case, but the fits were not significantly different from those with $\tilde{M}_{q,2}$.

[8] CLEO [42] has recently measured the $D^{*+}$ width, which gives, using lowest order $\chi$PT, a $D$-$D^*$-$\pi$ coupling $g^2 \approx 0.35$. However, NLO $\chi$PT and the $D^* \to D\pi$ decay gives $g^2 \approx 0.07$ [43]; while NLO $\chi$PT on the $D^{*+}$ width [Eq. (21) in [43]] gives $g^2 \approx 0.22$. A recent lattice computation [44] gives $g^2 \approx 0.45$. There is also some uncertainty in going from the $D$ to the $B$ system.

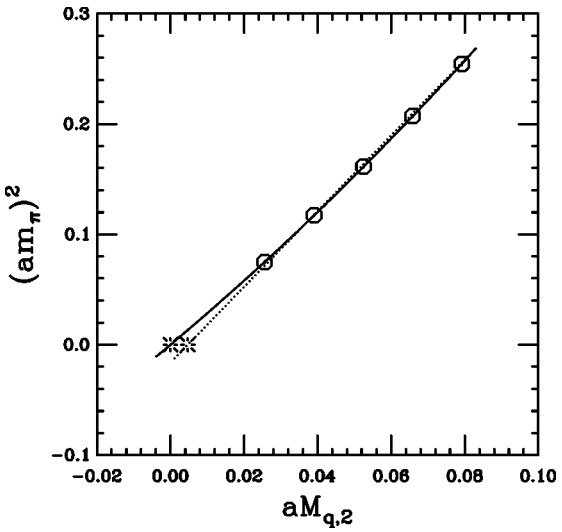


FIG. 5. $(am_\pi)^2$ vs $a\tilde{M}_{q,2}$ for set CP1. The solid line is a quadratic fit; the dotted line, the alternative linear fit. The fits have $\chi^2_{\rm cut}$/d.o.f.=0.06 and 36.5, respectively, with $\lambda_{\rm cut}=1$. The bursts are the extrapolated points where $(am_\pi)^2=0$.

Figure 5 shows the chiral extrapolation of $m_\pi^2$ to find $\kappa_c$, with both linear and quadratic fits. Since the independent variable, $\tilde{M}_{q,2}$, itself depends on $\kappa_c$, such fits have to be iterated two or three times to find a self-consistent value of $\kappa_c$ where both $m_\pi^2$ and $\tilde{M}_{q,2}$ vanish. This has been done only for the quadratic fit in Fig. 5 to emphasize the difference with the linear fit.

Table III shows the results for $\kappa_c$ and $\chi^2_{\rm cut}$ values for all the data sets. Note that the linear fits are uniformly very poor; while quadratic fits are quite good wherever there are enough light masses to compute a $\chi^2_{\rm cut}$. Although using $am_0$ as the independent variable actually reduces the $\chi^2_{\rm cut}$ values of the linear fits somewhat, they remain very poor. These features agree with what was found in Ref. [4]. We therefore use only quadratic fits/solves from here on for $m_\pi^2$ vs $a\tilde{M}_{q,2}$. Table IV gives the values of $\kappa_s$ resulting from these fits.

The case of $f_{qq}$ vs $a\tilde{M}_{q,2}$ is a more difficult one. Figures 6 and 7, and Table V show the extrapolations. Although the linear fits in both figures appear reasonable to the eye, that in Fig. 7 has a rather high value of $\chi^2_{\rm cut}$/d.o.f. as do many of the other linear fits in Table V. Where comparisons can be made, the quadratic fits are better. On the other hand, the quadratic fits often have quite large statistical errors, especially in the Wilson case where there are only three light quark masses. Furthermore, on the sets with the finest lattice spacings (C, CP, D, H, G, R, CP1, J) the linear fits are generally acceptable (set R is an exception). For these reasons, we use the linear fits for the central values and take the quadratic fits to estimate the ''standard chiral systematic error.'' As mentioned above, the fits in future work [45] will include chiral logs as well as quadratic terms.

Figure 8 shows a typical linear extrapolation of the light-light vector mass to the physical point for up/down quarks. As seen in Table V, the linear fits are almost always quite good, and we use the scale set with $m_\rho$ in this way as an alternative to that from $f_\pi$. The same fits also give an alternative value for $\kappa_s$, using $m_\phi$. The results are shown in Table IV.

Sample chiral fits for heavy-light masses and decay constants are shown in Figs. 9 and 10. Although the extrapolated data for all the sets are too extensive to tabulate here, they are available at http://www.physics.wustl.edu/~cb/Nf=2_tables, in the files ''*name*_chiral_mass.dat'' and ''*name*_chiral_fsqrtM.dat.'' In the latter files we give $f_{Qq}\sqrt{M_{Qq}}$, rather than $f_{Qq}$, because $f_{Qq}\sqrt{M_{Qq}}$ is what we will need later to extrapolate/interpolate to the mass of the *B* and *D* mesons. For the decay constants from sets CP1 and J, ''*name*'' includes the qualification NP-IOY or NP-tad because $f_{Qq}$ will of course depend on how the renormalization is done.

For almost all data sets, the linear chiral fits of the heavy-light masses are quite good, at least in the important range of meson masses between the *D* and the *B*. Sets L and T are exceptions, which is perhaps not surprising since their correlators are quite noisy to begin with, making it difficult to find good plateaus. Indeed, for set T the data are noisy enough that covariant chiral fits for heavy-light masses did not converge, with any choice for $\lambda_{\rm cut}$ except $\lambda_{\rm cut}=\infty$, i.e., noncovariant fits. However, since the linear fits to heavy-light masses were fine on the vast majority of the sets, we believe it is reasonable to use them exclusively. Linear fits to the static-light masses are always acceptable.

The situation for the heavy-light decay constants is similar to that for the light-light decay constants. Again, there is a small amount of curvature in these plots, and the direction of curvature is the same as for the light-light case. (Compare Fig. 10 with Figs. 6 and 7.) Therefore, quadratic chiral fits of $f_{Qq}$ are better than linear ones where the comparison can be made, but, as before, the quadratic fits/solves lead to significantly larger statistical errors. The main difference with the light-light case is that the linear fits typically improve as the mass of the heavy quark increases, so that by the time the physical *b* quark mass is reached they are generally quite reasonable. The only exceptions to this rule are the sets CP, for which linear fits are poor over the whole heavy-quark mass range, and T, which is noisy and again requires noncovariant fits. In the static-light case, linear fits are always good. We thus choose linear fits everywhere for the central values but use quadratic fits for the heavy-lights in estimating the systematic error in the standard chiral extrapolation. As discussed above, we expect that extrapolating both light-light and heavy-light fits in the same way will cancel at least some of the systematic error associate with curvature and chiral logarithms. Therefore, we change from linear to quadratic fits in both cases at once when we make our estimate of the ''standard'' chiral error.

To summarize: For central values, we use quadratic chiral fits in $a\tilde{M}_{q,2}$ for $m_\pi^2$ and linear fits for heavy-light and static-light masses and all the decay constants. We call this combination ''chiral choice I.'' Our standard chiral systematic errors are found by comparing the central values with the

TABLE III. Extrapolations of $a^2m_\pi^2$ vs $a\tilde{M}_{q,2}$ to find $\kappa_c$. When the number of degrees of freedom is 0 (quadratic fit with 3 $\kappa$ values), a solver is used instead of a fitter. For fits, the cutoff on correlation matrix eigenvalues ($\lambda_{\rm cut}$) is 1. For set 5.7-large, which consists of several lattice sizes, the central value is the average over all sets, the error is a combined weighted error, and the $\chi^2$ and d.o.f. shown are the ones from the volume $20^3\times 48$. See Sec. V B for a description of the fat-link computations.

| Name | $\kappa_c$ | $\chi^2_{\rm cut}$ | d.o.f. | $\kappa_c$ | $\chi^2_{\rm cut}$ | d.o.f. |
|---|---|---|---|---|---|---|
| | quadratic fit | | | linear fit | | |
| | | | quenched Wilson | | | |
| A | 0.169433(237) | — | 0 | 0.168607(89) | 29.3 | 1 |
| B | 0.169340(100) | — | 0 | 0.168383(52) | 227.0 | 1 |
| 5.7-large | 0.169748(24) | 0.3 | 2 | 0.168862(33) | 703.3 | 3 |
| E | 0.161397(124) | — | 0 | 0.161046(89) | 20.1 | 1 |
| C | 0.157228(95) | — | 0 | 0.156778(46) | 62.5 | 1 |
| CP | 0.157274(74) | — | 0 | 0.156906(25) | 44.0 | 1 |
| D | 0.151825(55) | — | 0 | 0.151663(35) | 28.0 | 1 |
| H | 0.149368(20) | — | 0 | 0.149248(15) | 18.9 | 1 |
| | | | $N_f=2$ Wilson | | | |
| L | 0.169422(61) | — | 0 | 0.168160(50) | 299.4 | 1 |
| N | 0.169515(56) | — | 0 | 0.168513(25) | 496.4 | 1 |
| O | 0.167197(41) | — | 0 | 0.166483(30) | 306.8 | 1 |
| M | 0.165919(59) | — | 0 | 0.165211(33) | 192.3 | 1 |
| P | 0.165257(47) | — | 0 | 0.164864(28) | 144.5 | 1 |
| U | 0.163065(27) | — | 0 | 0.162570(16) | 426.6 | 1 |
| T | 0.161528(22) | — | 0 | 0.161887(27) | 155.9 | 1 |
| S | 0.161400(20) | — | 0 | 0.160802(12) | 447.2 | 1 |
| G | 0.161158(72) | — | 0 | 0.160821(45) | 38.7 | 1 |
| R | 0.161167(23) | — | 0 | 0.160798(12) | 328.9 | 1 |
| | | | quenched clover | | | |
| CP1 | 0.135342(18) | 0.1 | 2 | 0.135168(8) | 109.4 | 3 |
| J | 0.135862(20) | 0.0 | 2 | 0.135792(16) | 45.8 | 3 |
| | | | fat-link clover ($N=10,\ c=0.045$) | | | |
| CPF | 0.125558(22) | 0.2 | 2 | — | — | — |
| RF | 0.125666(25) | — | 0 | — | — | — |

results of ''chiral choice II'': quadratic fits for $m_\pi^2$ and both light-light and heavy-light decay constants, and linear fits for heavy-light masses and static-light masses and decay constants. For the light-light vector meson masses, which enter only in various systematic error estimates (alternative scale determination from $m_\rho$, alternative $\kappa_s$ determination from $m_\phi$), we always use linear fits.

### E. Chiral logarithm effects

The standard chiral systematic error just described does not *directly* take into account the sharp curvature in decay constants at very small quark mass caused by terms of the form $-m_\pi^2\ln(m_\pi^2)$ in Eqs. (37) and (38). Putting aside the issue of scale choice, an extrapolation in the full theory that ignores the chiral log in $f_{Qq}$ is expected to overestimate $f_B$ and underestimate $f_{B_s}/f_B$ [8] (since $-m_\pi^2\ln m_\pi^2$ is concave down with rapid variation at small mass). However, because we set the scale with $f_\pi$ and use the same extrapolations for $f_{qq}$ and $f_{Qq}$, the effect on the individual decay constants is less clear. Even ratios such as $f_{B_s}/f_B$ are affected indirectly by the scale choice, through the fixing of $\kappa_s$, the hopping parameter for the strange quark. (Fixing $\kappa_b$, the bottom quark hopping parameter, has little effect on the ratio but does represent another scale effect on the individual decay constants.) It is easy to see that our scale choice should push $f_B$ and $f_{B_s}/f_B$ in the opposite direction of the $f_{Qq}$ extrapolation. We can thus hope that such effects largely cancel, and this is a justification for taking our central values and errors from the standard linear and quadratic chiral fits described in the previous section.

However, to test the above assumption and estimate the errors induced by not directly fitting with chiral log forms, we need alternative methods of evaluation that do not involve chiral extrapolations of individual decay constants. One approach that takes advantage of the fact that the chiral logs in $f_B$ and $f_\pi$ are similar in magnitude is to perform chiral extrapolations only on the ratio $f_B/f_\pi$ (more precisely, $f_{Qq}/f_{qq}$). Given the expected range for the parameter $g^2$, the

TABLE IV. Values of $\kappa_s$, the hopping parameter of the strange quark, from fits to the light-light pseudoscalars and vectors. In the former case, we adjust the pseudoscalar mass to $\sqrt{2m_K^2-m_\pi^2}$; in the latter, we adjust the vector mass to $m_\phi$. The values of $\chi^2$ and degrees of freedom can be found by referring to the corresponding fits in Tables III and V. Data from set 5.7-large are combined as in Table III. See Sec. V B for a description of the fat-link computations.

| Name | $\kappa_s$ (pseudoscalars) quadratic fit | $\kappa_s$ (vectors) linear fit |
|---|---|---|
| | quenched Wilson | |
| A | 0.164331(432) | 0.163173(407) |
| B | 0.163629(355) | 0.163709(215) |
| 5.7-large | 0.163916(100) | 0.163456(78) |
| E | 0.158203(170) | 0.157729(351) |
| C | 0.154567(97) | 0.154780(229) |
| CP | 0.154857(99) | 0.154638(152) |
| D | 0.150395(66) | 0.150316(102) |
| H | 0.148415(42) | 0.148322(87) |
| | $N_f=2$ Wilson | |
| L | 0.164114(201) | 0.164064(184) |
| N | 0.164436(213) | 0.164027(202) |
| O | 0.162938(121) | 0.162691(120) |
| M | 0.161778(205) | 0.161830(206) |
| P | 0.161518(141) | 0.161374(106) |
| U | 0.159690(81) | 0.159373(103) |
| T | 0.158610(121) | 0.157243(148) |
| S | 0.158633(68) | 0.158423(50) |
| G | 0.158795(94) | 0.158350(146) |
| R | 0.158736(55) | 0.158465(85) |
| | quenched clover | |
| CP1 | 0.133882(41) | 0.133515(63) |
| J | 0.134665(45) | 0.134400(56) |
| | fat-link clover ($N=10$, $c=0.045$) | |
| CPF | 0.123206(46) | 0.123481(137) |
| RF | 0.123440(62) | 0.123236(162) |

ratio has a chiral log term of opposite sign from that of $f_B$ alone and either comparable or greatly reduced magnitude [see Eqs. (37) and (38) and the footnote shortly before]. In practice, since the slope of $f_{qq}$ is greater than $f_{Qq}$, $f_{qq}/f_{Qq}$ is more linear than $f_{Qq}/f_{qq}$, and we work with the former.

Figure 11 shows a chiral extrapolation of $f_{qq}/f_{Qq}$ for set R, with $\kappa_Q$ chosen so that $M_{Qq}$ is near the $B$ mass. There is clear curvature, so a linear fit is not appropriate, and we fit (solve) quadratically. To the extent that a residual chiral log remains in the ratio, the quadratic fit should somewhat overestimate $f_\pi/f_B$ and hence also $f_{B_s}/f_B$.

However, to take real advantage of the presumed reduction of chiral logs in $f_\pi/f_B$ and known sign of the error in $f_{B_s}/f_B$, we must eliminate the dependence of the scale and $\kappa_s$ on a chiral extrapolation. This means that common scale choices such as $f_\pi$, $m_\rho$ or $m_N$ cannot be used. Further, we are reluctant to employ static potential quantities such as the string tension, $r_0$, or $r_1$, because their physical values are only known phenomenologically, with uncertain errors. Instead, we look at three more-or-less physical quantities associated with the $s$ quark: the vector meson mass $m_\phi$, and the mass and decay constant of a would-be $s\bar{s}$ pseudoscalar, $m_{ss}$ and $f_{ss}$. To be precise, the $s\bar{s}$ meson is made of two valence quarks with the physical strange quark mass, but in a standard sea quark background: either the physical $N_f=3$ case (with $m_u=m_d=\hat{m}^{\rm phys}$ and $m_s^{\rm phys}$), or, corresponding more closely to our simulations, the $N_f=2$ case (with $m_u=m_d$

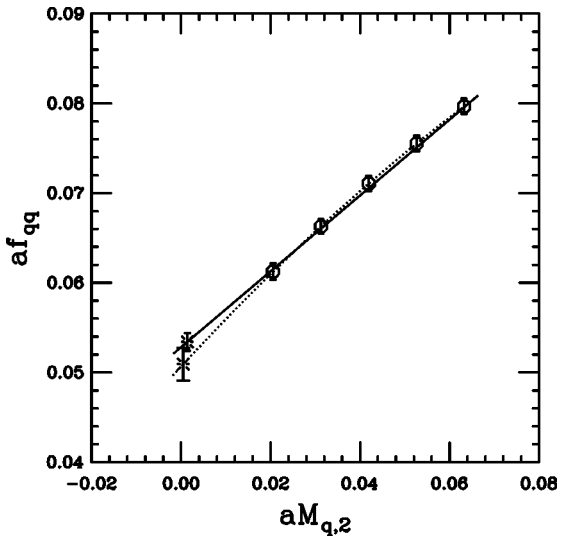


FIG. 6. The light-light pseudoscalar decay constant, $f_{qq}$, vs $a\tilde{M}_{q,2}$ for set *J*. The solid line is a linear fit; the dotted line, the alternative quadratic fit. The fits have $\chi^2_{\rm cut}$/d.o.f.$=1.1$ and 0.005, respectively, with $\lambda_{\rm cut}=1$ (1 eigenvector of 5 kept). The bursts are the extrapolated points where $\tilde{M}_{q,2}$ takes its physical value (i.e., $\kappa=\kappa_{u,d}$). The burst on the dotted line has been displaced slightly for clarity.

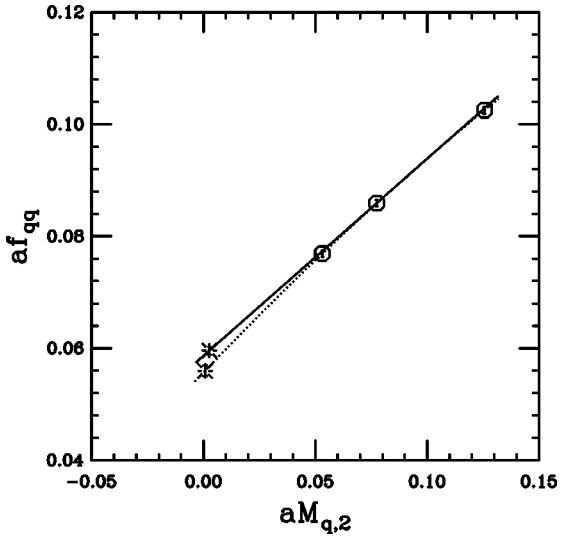


FIG. 7. Same as Fig. 6, but for set R. The linear fit (solid line) has $\chi^2_{\rm cut}$/d.o.f.$=8.7$, $\lambda_{\rm cut}=1$ (1 eigenvector of 3 kept); while the quadratic fit (dotted line) has no degrees of freedom.

TABLE V. Extrapolations of $af_{qq}$ and $m_\rho$ vs $a\tilde{M}_{q,2}$ to find the scale, $a^{-1}$, using $f_\pi = 0.1307$ GeV and $m_\rho = 0.768$ GeV. When the number of degrees of freedom is 0 (quadratic fit with 3 $\kappa$ values), a solver is used instead of a fitter. For fits, the cutoff on correlation matrix eigenvalues ($\lambda_{\rm cut}$) is 1. Data from set 5.7-large are combined as in Table III. See Sec. V B for a description of the fat-link computations.

| Name | $a^{-1}$ (GeV) | $\chi^2_{\rm cut}$ | d.o.f. | $a^{-1}$ (GeV) | $\chi^2_{\rm cut}$ | d.o.f. | $a^{-1}$ (GeV) | $\chi^2_{\rm cut}$ | d.o.f. |
|---|---|---|---|---|---|---|---|---|---|
| | $f_{qq}$, linear fit | | | $f_{qq}$, quadratic fit | | | $m_\rho$, linear fit | | |
| | | | | quenched Wilson | | | | | |
| A | 1.391(66) | 5.3 | 1 | 1.586(122) | — | 0 | 1.413(32) | 1.5 | 1 |
| B | 1.311(48) | 6.1 | 1 | 1.453(66) | — | 0 | 1.488(25) | 0.0 | 1 |
| 5.7-large | 1.339(14) | 3.3 | 3 | 1.388(17) | 0.3 | 2 | 1.450(8) | 9.9 | 3 |
| E | 1.780(43) | 3.4 | 1 | 1.851(63) | — | 0 | 1.848(73) | 0.1 | 1 |
| C | 2.124(54) | 1.8 | 1 | 2.266(96) | — | 0 | 2.414(102) | 0.5 | 1 |
| CP | 2.211(48) | 1.2 | 1 | 2.339(124) | — | 0 | 2.333(51) | 0.2 | 1 |
| D | 3.151(91) | 2.8 | 1 | 3.331(111) | — | 0 | 3.389(108) | 0.2 | 1 |
| H | 4.388(121) | 0.5 | 1 | 4.490(146) | — | 0 | 4.489(150) | 0.0 | 1 |
| | | | | $N_f = 2$ Wilson | | | | | |
| L | 1.375(30) | 15.7 | 1 | 1.585(43) | — | 0 | 1.545(23) | 0.0 | 1 |
| N | 1.432(35) | 2.0 | 1 | 1.524(53) | — | 0 | 1.524(25) | 0.3 | 1 |
| O | 1.568(25) | 2.3 | 1 | 1.654(55) | — | 0 | 1.685(20) | 0.9 | 1 |
| M | 1.608(47) | 1.0 | 1 | 1.680(56) | — | 0 | 1.789(37) | 0.3 | 1 |
| P | 1.713(38) | 2.0 | 1 | 1.773(50) | — | 0 | 1.853(22) | 2.3 | 1 |
| U | 1.800(25) | 3.2 | 1 | 1.868(34) | — | 0 | 1.888(25) | 0.3 | 1 |
| T | 1.800(37) | 24.3 | 1 | 1.939(40) | — | 0 | 1.839(20) | 0.7 | 1 |
| S | 2.038(28) | 7.6 | 1 | 2.192(31) | — | 0 | 2.157(19) | 0.5 | 1 |
| G | 2.243(38) | 4.3 | 1 | 2.377(63) | — | 0 | 2.242(52) | 0.0 | 1 |
| R | 2.194(26) | 8.7 | 1 | 2.306(39) | — | 0 | 2.269(31) | 3.6 | 1 |
| | | | | quenched clover | | | | | |
| CP1 | 1.994(29) | 8.0 | 3 | 2.093(65) | 3.9 | 2 | 1.908(26) | 0.2 | 3 |
| J | 2.447(45) | 3.3 | 3 | 2.545(90) | 0.0 | 2 | 2.383(39) | 1.4 | 3 |
| | | | | fat-link clover ($N = 10$, $c = 0.045$) | | | | | |
| CPF | 1.847(18) | 14.4 | 3 | 1.923(28) | 0.5 | 2 | 2.114(61) | 6.1 | 3 |
| RF | 1.873(27) | 1.4 | 1 | 1.939(69) | — | 0 | 1.920(47) | 0.3 | 1 |

$=\hat{m}^{\rm phys}$). Here the superscript ''phys'' stands for the physical mass, and we neglect isospin violations as usual.

The quantity $f_{ss}$ can be related to $f_K$ and $f_\pi$ in 1-loop (NLO) partially quenched chiral perturbation theory (PQ$\chi$PT), in a manner independent of the analytic $p^4$ (''Gasser-Leutwyler'') constants. Using the formulas in Refs. [48] and [49] for $N_f = 2$ and $N_f = 3$, respectively, we find

$$\frac{f_{ss}^{(2)} f_\pi}{f_K^2} = 1 + \frac{1}{16\pi^2 f^2}\left[\tfrac{1}{2} m_\pi^2 \ln(m_{ss}^2/m_\pi^2) - \tfrac{1}{2} m_{ss}^2 + \tfrac{1}{2} m_\pi^2\right] \approx 0.93 \tag{39}$$

$$\frac{f_{ss}^{(3)} f_\pi}{f_K^2} = 1 + \frac{1}{16\pi^2 f^2}\left[\tfrac{3}{2} m_\eta^2 \ln(m_\eta^2/\Lambda^2) - \tfrac{1}{2} m_\pi^2 \ln(m_\pi^2/\Lambda^2) - m_{ss}^2 \ln(m_{ss}^2/\Lambda^2)\right] \approx 0.95 \tag{40}$$

where, in the numerical evaluation, we have used $f = f_\pi = 130.7$ MeV and $m_{ss}^2 = \tfrac{3}{2} m_\eta^2 - \tfrac{1}{2} m_\pi^2$. (The latter relation is

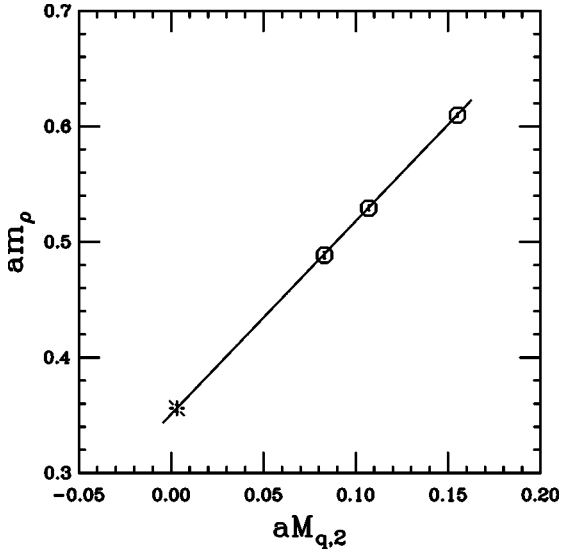


FIG. 8. Linear extrapolation of the light-light vector meson mass to the physical point ($\rho$ meson, indicated by the burst). The data are from set S. The fit has $\chi^2_{\rm cut}/{\rm d.o.f.} = 0.5$ with $\lambda_{\rm cut} = 1$.

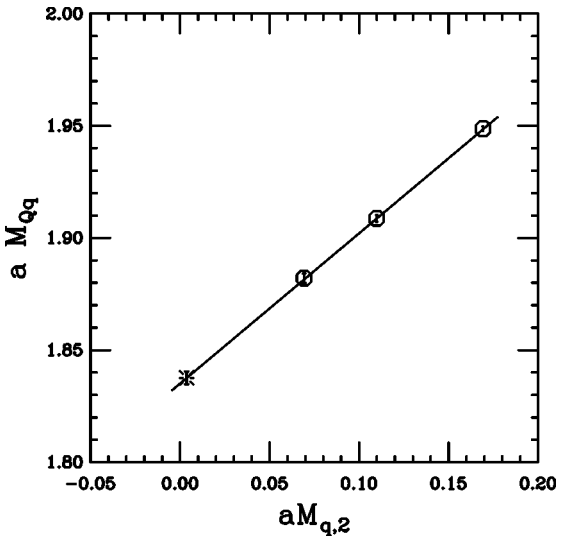


FIG. 9. Linear chiral extrapolation of the heavy-light pseudoscalar meson mass, to the physical point ($\kappa=\kappa_{u,d}$, indicated by the burst). The data are from set U, $\kappa_Q=0.113$. The fit has $\chi^2_{\rm cut}$/d.o.f. $=0.7$ with $\lambda_{\rm cut}=1$.

theoretically convenient here because it makes Eq. (40) explicitly independent of the chiral scale $\Lambda$.)

For $m_{ss}$, we consider a few choices. Two tree level relations have already been mentioned:

$$m_{ss}^2=2m_K^2-m_\pi^2 \tag{41}$$

$$m_{ss}^2=\tfrac{3}{2}m_\eta^2-\tfrac{1}{2}m_\pi^2. \tag{42}$$

With Refs. [48,49], we can also derive 1-loop relations for $m_{ss}$ similar to Eqs. (39) and (40), although they do involve

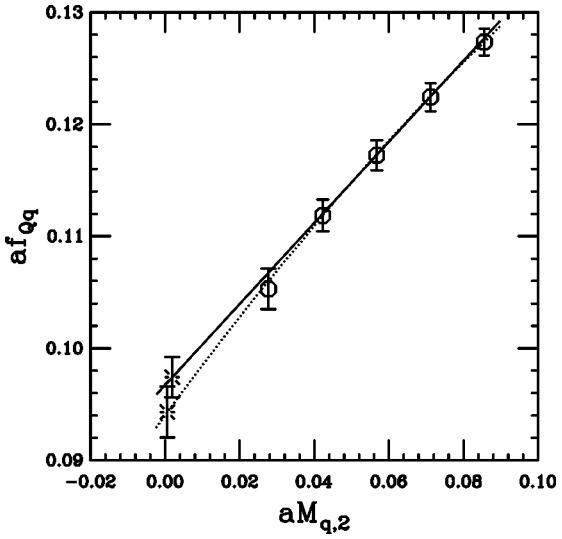


FIG. 10. Linear (solid) and quadratic (dotted) chiral extrapolations of $f_{Qq}$ to the physical point ($\kappa=\kappa_{u,d}$ indicated by the bursts). The data are from set CP1, $\kappa_Q=0.09$, with NP-IOY renormalization. The linear fit has $\chi^2_{\rm cut}$/d.o.f.$=1.0$; the quadratic, 0.3. The parameter $\lambda_{\rm cut}=1$ in both cases. The burst on the dotted line has been displaced slightly for clarity.

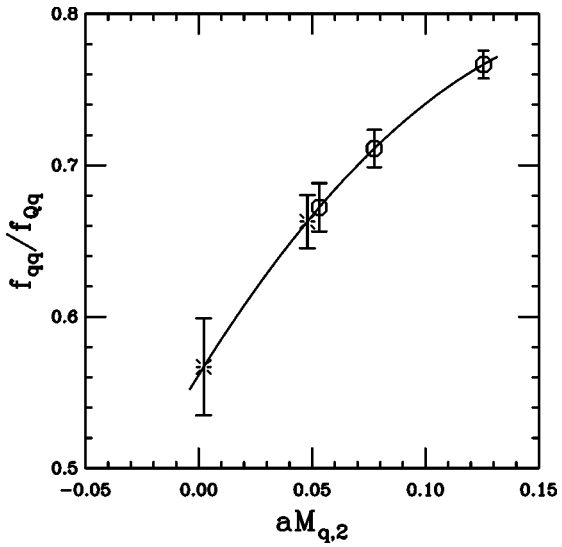


FIG. 11. Quadratic chiral extrapolation of $f_{qq}/f_{Qq}$ from set R, with $\kappa_Q=0.125$. The bursts show the extrapolation to $\kappa_s$ and $\kappa_{u,d}$, with these values determined by method 6 in Table VI.

analytic terms indirectly through the quark mass ratios. In particular, we use the $N_f=2$ result:

$$\frac{m_{ss}^2m_\pi^2}{m_K^4}=\frac{4\hat{m}/m_s}{(1+\hat{m}/m_s)^2}\times\left[1+\frac{1}{16\pi^2f^2}[-m_\pi^2\ln(m_{ss}^2/m_\pi^2)+m_{ss}^2-m_\pi^2]\right]\approx 0.17, \tag{43}$$

where we have taken $m_s/\hat{m}=24.4$ [50].

We then perform a series of analyses. For each, we choose 2 of the quantities $f_{ss}$, $m_{ss}$, and $m_\phi$, and a method of evaluation for the ''physical'' quantities $f_{ss}$ [either Eq. (39) or Eq. (40)] and/or $m_{ss}$ [either Eq. (41), Eq. (42) or Eq. (43)]. We then fit the ratio of the 2 chosen quantities as a function of light quark mass ($a\tilde{M}_{q,2}$) in order to determine $\kappa_s$. Generally, only an interpolation or mild extrapolation is required. Figures 12 and 13 show two examples of such fits, for $m_{ss}/f_{ss}$ and $m_{ss}/m_\phi$, respectively. The former uses Eqs. (41) and (39); while the latter, Eq. (43). Note that a slight extrapolation is required to find $\kappa_s$ in Fig. 12. In Fig. 13, $\kappa_s$ is determined by an interpolation, which is more similar to the standard analysis. The difference between the two situations gives some indication of the errors of the procedure. In Table VI we show the results for $\kappa_s$ for 12 different versions of such fits, performed on two different dynamical sets of configurations (the ones with the lightest sea quark masses).

Given $\kappa_s$, the next step is to determine the scale, $a^{-1}$. We consider one of the two quantities in the ratio used to determine $\kappa_s$, extrapolate or interpolate as needed to reach $\kappa=\kappa_s$, and set the result to the ''physical'' value of that quantity. The results from either of the two quantities in the ratio should be consistent; they are. Figure 14 shows a quadratic extrapolation of $f_{qq}$ to $\kappa_s$; $a^{-1}$ is fixed from the result via

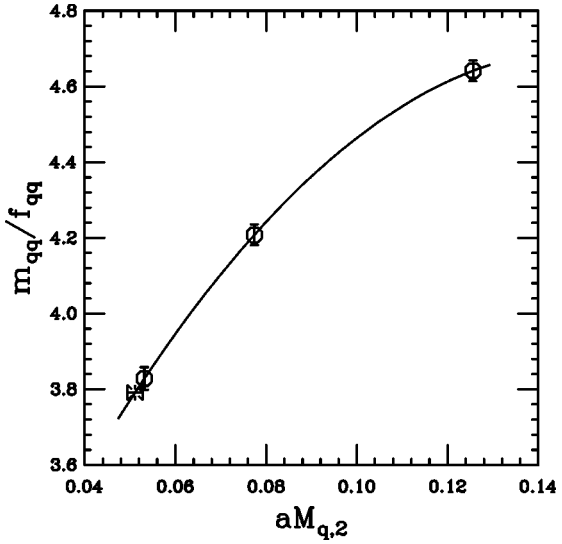


FIG. 12. Quadratic extrapolation of $m_{qq}/f_{qq}$ to $m_{ss}/f_{ss}$ on set R, with $m_{ss}$ from Eq. (41) and $f_{ss}$ from Eq. (39). The abscissa of the burst gives the value of the quark mass, $aM_{q,2}$, at $\kappa_s$. This particular determination is called ''method 1'' (see text and Table VI).

Eq. (39). Although an extrapolation is again required in this particular case, it is only over a short distance in quark mass.

Once the scale is determined, the standard extrapolation of $m_{qq}^2$ produces the light quark hopping parameter, $\kappa_{u,d}$. It is, of course, very close to $\kappa_c$ in all cases.

Results for various scale determinations are shown in Table VI. In most cases, the values of $a^{-1}$ are significantly larger than those from the standard linear (or quadratic) extrapolation of $f_\pi$ (see Table V). This is not unexpected because extrapolation from relatively large mass without the chiral log term in Eq. (38) should overestimate $af_\pi$. Further, other lattice spacing determinations from light quark physics (e.g., $m_\rho$, $m_N$) also typically involve linear or quadratic chiral extrapolations from rather high masses, so their generally good agreement with the standard $f_\pi$ scale cannot be used to rule out the results in Table V. Indeed, it has been known for some time that heavy quark physics (charmonium or upsilonium) typically gives scales $\sim 10$ to 20 % larger than light quark physics. (For a recent example, see Table I in Ref. [51].) It now appears that at least some of this discrepancy is due to the extrapolation in the light quark mass.

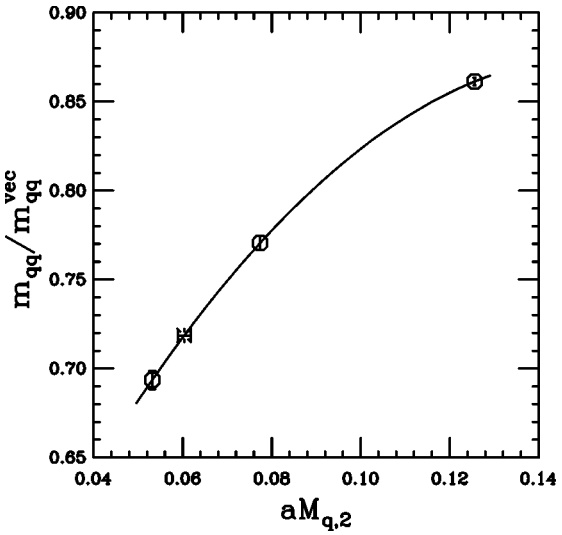


FIG. 13. Quadratic interpolation of $m_{qq}/m_{qq}^{\rm vec}$ to $m_{ss}/m_\phi$ on set R, with $m_{ss}$ from Eq. (43). The abscissa of the burst gives the value of the quark mass, $aM_{q,2}$, at $\kappa_s$. This particular determination is called ''method 8'' (see text and Table VI).

On the other hand, the result for $a^{-1}$ is unreasonably large ($\gtrsim 30\%$ bigger than the central value) in three cases in Table VI. (In all other cases the scale is at most 17% greater than the central value.) The three cases also have long extrapolations to find $\kappa_s$ (i.e., a value of $\kappa_s$ very close to $\kappa_c$—compare Table III) and very large statistical errors in both $\kappa_s$ and $a^{-1}$. These cases are marked with asterisks and are omitted from any averages of decay constant effects.

Given $\kappa_s$, $\kappa_{u,d}$, and $a^{-1}$, the ratio $f_{qq}/f_{Qq}$ can now be interpolated/extrapolated as in Fig. 11 to $\kappa_s$ and $\kappa_{u,d}$. Using the physical $f_\pi$ and the relevant choice for $f_{ss}$, this produces $f_{Qs}$ or $f_{Qu,d}$, which are then interpolated in heavy quark mass in the same way as in our standard analysis, described in the next section. The differences of the final decay constants from the central values are displayed in Table VI for each of the methods. These differences will be used in Sec. V D to estimate the effects of chiral logs in the dynamical case. We also explain there why we think it would be inappropriate at this stage to *correct* the central values by the chiral log effects. Instead we use the changes shown in Table VI only to estimate the systematic error.

### F. Interpolations in heavy quark mass

We proceed to compute physical decay constants such as $f_B$ and $f_{B_s}$ for each lattice set. Our starting point is the values of $f_{Qq}\sqrt{M_{Qq}}$ (for $q=u,d$ or $q=s$) as functions of the heavy quark mass produced by the chiral fits of the previous two sections.

The static limit is also included where we have it. According to the heavy quark effective theory (HQET) [52], $f_{Qq}\sqrt{M_{Qq}}$ should depend on the heavy meson mass as a polynomial in $1/M_{Qq}$, up to logarithms. We therefore first divide out the one-loop logarithmic dependence of the decay constants in the heavy quark limit [53], producing what we call $f'_{Qq}\sqrt{M_{Qq}}$:

$$f'_{Qq}\sqrt{M_{Qq}} = \frac{f_{Qq}\sqrt{M_{Qq}}}{1+\alpha_V(q^*)\ln(aM_{Qq})/\pi}, \tag{44}$$

where we have ignored the difference between the heavy quark and heavy meson masses, and where $q^*$ takes the values discussed in Secs. II A and II B.

The data are now expressed in physical units, always using $f_\pi$ to set the scale for the central values. The quantity $f'_{Qq}\sqrt{M_{Qq}}$ is then plotted vs $1/M_{Qq}$, where $M_{Qq}$ is the kinetic meson mass $M_{Qq,2}$ defined in Eq. (8). We fit to a polynomial in $1/M_{Qq}$, interpolate to $m_B$, $m_{B_s}$, $m_D$ or $m_{D_s}$, and then replace the logarithm in Eq. (44), evaluated at the appropriate meson mass. These are always interpolations, not

TABLE VI. Values of $\kappa_s$ and $a^{-1}$ (in GeV) for various methods of the analysis that do not require (long) chiral extrapolation. For each method, the upper entry is from set R; the lower, from set P. These should be compared with our central values, which come from linear chiral extrapolation of $f_{qq}$ (and quadratic interpolation of $m_{qq}^2$): $\kappa_s=0.15873(5)$, $a^{-1}=2.19(3)$ GeV (set R), and $\kappa_s=0.16152(14)$, $a^{-1}=1.71(4)$ GeV (set P). We also show the changes (in MeV) from central values that each method produces in decay constants, as well as the average and standard devation of the mean of those changes. These quantities are used in Sec. V D to estimate the systematic effects of chiral logarithms. Lines for which $a^{-1}$ differs by more than 20% from the central value (indicated by "*") are considered unreliable and are eliminated from the averages.

| Method | Description | $\kappa_s$ | $a^{-1}$ | $f_B$ | $f_{B_s}$ | $f_D$ | $f_{D_s}$ |
|---|---|---|---|---|---|---|---|
| 1 | $\kappa_s$: $m_{ss}/f_{ss}$; $a$: $f_{ss}$ | 0.15909(7) | 2.38(4) | +11 | +17 | +2 | +6 |
| | $m_{ss}$: Eq. (41); $f_{ss}$: Eq. (39) | 0.16137(15) | 1.68(4) | −3 | −7 | +7 | −12 |
| 2 | $\kappa_s$: $m_{ss}/f_{ss}$; $a$: $f_{ss}$ | 0.15926(7) | 2.48(4) | +13 | +28 | +0 | +13 |
| | $m_{ss}$: Eq. (41); $f_{ss}$: Eq. (40) | 0.16166(14) | 1.76(4) | −2 | +3 | +6 | −4 |
| 3 | $\kappa_s$: $m_{ss}/f_{ss}$; $a$: $f_{ss}$ | 0.15847(8) | 2.22(3) | +8 | +5 | +4 | −3 |
| | $m_{ss}$: Eq. (43); $f_{ss}$: Eq. (33) | 0.16024(22) | 1.55(4) | −7 | −21 | +7 | −21 |
| 4 | $\kappa_s$: $m_{ss}/f_{ss}$; $a$: $f_{ss}$ | 0.15937(7) | 2.47(4) | +13 | +24 | +1 | +10 |
| | $m_{ss}$: Eq. (42) ; $f_{ss}$: Eq. (39) | 0.16185(14) | 1.75(4) | −2 | −1 | +6 | −7 |
| 5 | $\kappa_s$: $m_{ss}/f_{ss}$; $a$: $f_{ss}$ | 0.15953(7) | 2.57(4) | +15 | +34 | −1 | +17 |
| | $m_{ss}$: Eq. (42) ; $f_{ss}$: Eq. (40) | 0.16211(13) | 1.83(5) | −0 | +9 | +5 | +0 |
| 6 | $\kappa_s$: $m_{ss}/m_\phi$; $a$: $m_\phi$ | 0.15922(6) | 2.46(4) | +13 | +21 | +1 | +7 |
| | $m_{ss}$: Eq. (41) ; $f_{ss}$: Eq. (39) | 0.16232(7) | 1.96(2) | +3 | +11 | +4 | −2 |
| 7 | $\kappa_s$: $m_{ss}/m_\phi$; $a$: $m_\phi$ | 0.15922(6) | 2.46(4) | +13 | +27 | +1 | +13 |
| | $m_{ss}$: Eq. (41) ; $f_{ss}$: Eq. (40) | 0.16232(7) | 1.96(2) | +3 | +16 | +4 | +4 |
| 8 | $\kappa_s$: $m_{ss}/m_\phi$; $a$: $m_\phi$ | 0.15871(6) | 2.33(3) | +10 | +10 | +3 | −0 |
| | $m_{ss}$: Eq. (43) ; $f_{ss}$: Eq. (39) | 0.16170(7) | 1.89(2) | +1 | +3 | +5 | −9 |
| 9 | $\kappa_s$: $m_{ss}/m_\phi$; $a$: $m_\phi$ | 0.15946(6) | 2.53(4) | +14 | +27 | −1 | +11 |
| | $m_{ss}$: Eq. (42) ; $f_{ss}$: Eq. (39) | 0.16262(7) | 2.00(3) | +3 | +15 | +3 | +2 |
| 10 | $\kappa_s$: $m_{ss}/m_\phi$; $a$: $m_\phi$ | 0.15946(6) | 2.53(4) | +14 | +32 | −1 | +17 |
| | $m_{ss}$: Eq. (43) ; $f_{ss}$: Eq. (40) | 0.16262(7) | 2.00(3) | +3 | +20 | +3 | +8 |
| * 11 | $\kappa_s$: $f_{ss}/m_\phi$; $a$: $f_{ss}$ | 0.16034(107) | 2.83(47) | +18 | +48 | −5 | +27 |
| * | $f_{ss}$: Eq. (39) | 0.16479(71) | 2.36(16) | +9 | +47 | −2 | +35 |
| 12 | $\kappa_s$: $f_{ss}/m_\phi$; $a$: $f_{ss}$ | 0.15881(80) | 2.35(21) | +11 | +17 | +3 | +6 |
| * | $f_{ss}$: Eq. (40) | 0.16420(67) | 2.25(14) | +7 | +42 | −0 | +31 |
| | **average** | | | +6 | +14 | +3 | +3 |
| | **standard deviation of mean** | | | 2 | 3 | 1 | 2 |

extrapolations, because we have either the static-light point (all Wilson sets) or heavy-light masses above the $B$ (the clover sets CP1 and J, using the Fermilab formalism).

For the quenched Wilson data, we do two versions of the polynomial fit: (i) a quadratic fit to heavy-light mesons in the approximate mass range 2 to 4 GeV plus the static-light meson ("heavier-heavies") and (ii) a quadratic fit to mesons in the approximate mass range 1.25 to 2 GeV plus the static-light meson ("lighter-heavies"). These fits keep just one eigenvector of the correlation matrix, which corresponds to $\lambda_{\rm cut}=0.9$ to 1.1. To estimate the effect of leaving out higher powers in $1/M_{Qq}$ in the fits, we also perform, for the central $q^*$ and chiral fit choices, fit (iii): a cubic fit to all the mesons in the range 1.25 to 4 GeV plus the static-light meson. The correlation matrix for fit (iii) typically has almost twice the number of eigenvectors as fits (i) and (ii), and we keep 2 of them. This corresponds to $\lambda_{\rm cut}=0.2$ to 1.0.

We make basically the same fits for the Wilson data on the dynamical lattices. The main difference is that we cut off fits (i) and (iii) at approximately 3, rather than 4, GeV. These lattices are almost all quite large, and, as explained in Sec. III A, we have trouble pulling out the lightest state for very heavy masses on large lattices with our approach to the hopping expansion. To make up for some of the points lost by

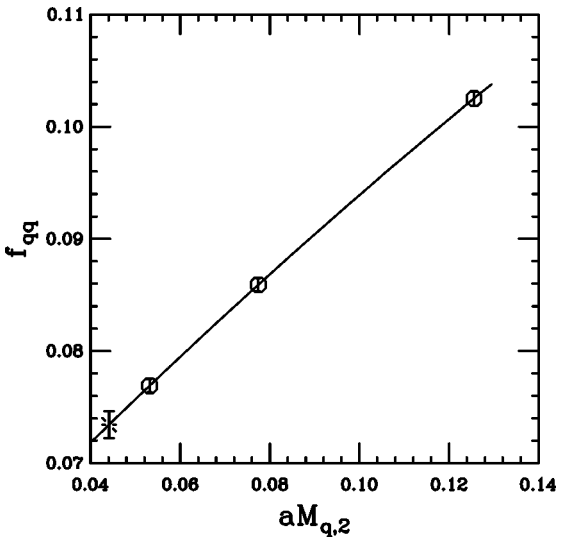


FIG. 14. Quadratic extrapolation on set R of $f_{qq}$ to $\kappa_s$, which in turn was found by extrapolation of $m_{ss}/f_{ss}$ using Eqs. (42) and (39). This is method 4 in Table VI.

the reduced upper cutoff on fit (i), we also reduce the lower cutoff slightly, to 1.8 GeV.

For the quenched clover sets, we make corresponding fits. However, the mass ranges are somewhat different because we have only five heavy quark values, do not have a static point, and, most importantly, use standard algorithms with FFT, facilitating the extraction of the lowest states even for very heavy masses. In this case, fit (i) (heavier-heavies) is a quadratic fit over the approximate meson mass range 2.3 to 6 GeV; while fit (ii) (lighter-heavies) is over the mass range 1.7 to 3 GeV.

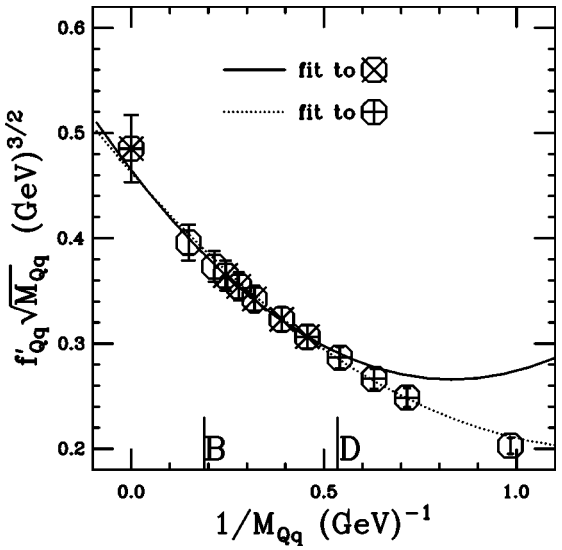


FIG. 15. $f'_{Qq}\sqrt{M_{Qq}}$ vs $1/M_{Qq}$ for set CP (quenched Wilson). The scale is set by $f_\pi$. The solid line is fit (1) (''heavier-heavies'') and includes points marked with a cross. The dotted line is fit (2) (''lighter-heavies'') and includes points marked with a plus. The fits have $\chi^2_{\rm cut}$/d.o.f.$=0.4$ and 0.9, respectively, with $\lambda_{\rm cut}=1$ (1 eigenvector kept).

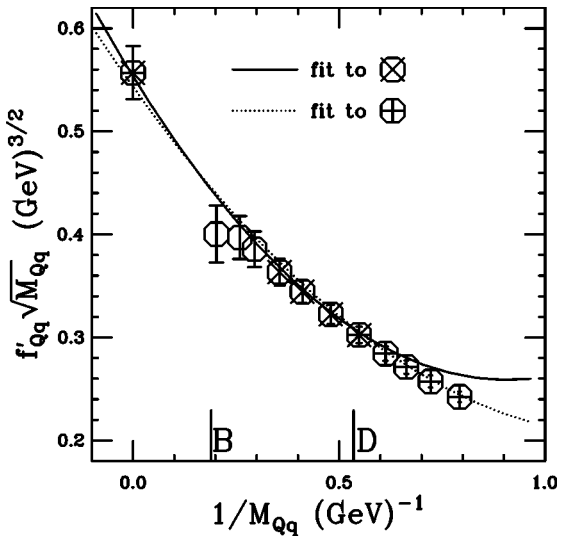


FIG. 16. Same as Fig. 15, but for set R (Wilson valence quarks on dynamical lattices). The solid line has $\chi^2_{\rm cut}$/d.o.f.$=0.2$; the dotted line, 0.3. The tail-off of $f'_{Qq}\sqrt{M_{Qq}}$ in the range $0.2\ {\rm GeV}^{-1} < 1/M_{Qq} < 0.3\ {\rm GeV}^{-1}$ is attributed to the difficulty in isolating asymptotic states for large masses and volumes—see text.

In central values, we use fit (i) for $f_B$ and $f_{B_s}$ and fit (ii) for $f_D$ and $f_{D_s}$. The alternative fits go into the systematic error estimates, as in Ref. [4]. However, for the central values of ratios involving both $B$ and $D$ mesons (i.e., $f_B/f_{D_s}$, $f_{B_s}/f_{D_s}$, and $f_B/f_D$), both numerators and denominators are taken from fit (ii). As explained in Sec. IV, this tends to reduce the estimate of the magnetic mass error.

Figures 15, 16, and 17 give examples of the behavior of $f'_{Qq}\sqrt{M_{Qq}}$ for the quenched Wilson, Wilson on dynamical

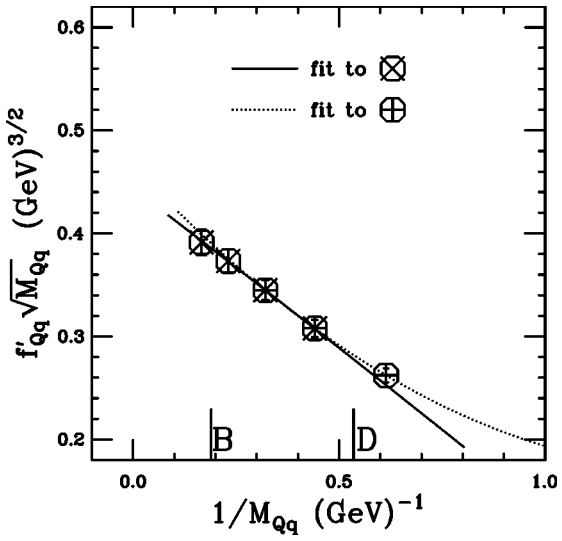


FIG. 17. Same as Fig. 15, but for set J (quenched clover), with NP-tad renormalization. The solid line has $\chi^2_{\rm cut}$/d.o.f.$=0.55$; the dotted line has no degrees of freedom. The solid line is slightly concave down, unlike the case in Figs. 15 and 16.

TABLE VII. Central values of decay constants, in MeV, for each data set. Statistical errors include the effect of changing the time ranges over which correlators are fit, as described in the text. For sets A and B, the values reported are those for which the light-light results ($\kappa_c$, $\kappa_s$, and $a^{-1}$) and their errors are taken from the averages over set 5.7-large.

| Name | $f_B$ | $f_{B_s}$ | $f_D$ | $f_{D_s}$ |
|---|---|---|---|---|
| | | quenched Wilson | | |
| A | 193.6(8.6) | 234.9(5.8) | 216.6(7.8) | 256.9(6.5) |
| B | 196.8(11.1) | 236.1(8.2) | 220.7(10.9) | 261.8(7.4) |
| E | 190.9(7.7) | 219.1(7.8) | 214.7(8.6) | 246.1(8.1) |
| C | 172.3(8.0) | 206.2(6.8) | 198.8(7.7) | 232.8(6.9) |
| CP | 177.0(7.8) | 210.8(6.4) | 206.7(6.4) | 238.2(5.7) |
| D | 174.9(7.5) | 199.8(6.5) | 206.8(7.9) | 232.5(6.3) |
| H | 180.6(12.1) | 206.7(10.8) | 206.6(10.9) | 232.9(9.0) |
| | | $N_f=2$ Wilson | | |
| L | 188.6(9.7) | 220.3(10.3) | 214.7(7.4) | 249.5(6.7) |
| N | 205.7(13.6) | 239.0(10.4) | 222.9(10.6) | 261.5(7.6) |
| O | 206.8(12.6) | 239.9(10.8) | 230.8(6.3) | 262.4(5.0) |
| M | 190.6(12.5) | 226.9(10.2) | 215.9(11.5) | 250.2(8.4) |
| P | 193.1(6.9) | 225.6(6.4) | 212.9(6.7) | 249.5(5.9) |
| U | 196.5(9.4) | 235.0(7.9) | 224.8(7.2) | 261.2(7.6) |
| T | 193.3(15.8) | 219.3(12.5) | 209.1(8.3) | 236.3(6.7) |
| S | 202.6(6.8) | 234.6(5.6) | 223.9(5.2) | 256.6(4.7) |
| G | 198.5(6.2) | 234.0(6.7) | 220.0(5.0) | 254.7(5.2) |
| R | 206.2(7.9) | 239.2(8.1) | 223.4(5.4) | 254.6(5.1) |
| | | quenched clover | | |
| CP1_NP-IOY | 184.1(5.7) | 212.8(4.4) | — | — |
| CP1_NP-tad | 176.1(5.2) | 203.4(3.9) | 196.3(3.7) | 220.0(2.8) |
| J_NP-IOY | 176.6(6.3) | 204.4(5.9) | — | — |
| J_NP-tad | 174.0(6.0) | 201.9(5.7) | 203.5(4.8) | 228.2(4.1) |

lattices, and quenched clover cases, respectively. Essentially all fits on all sets are acceptable. In Fig. 16, one can see the tail-off of $f'_{Qq}\sqrt{M_{Qq}}$ for large heavy quark masses ($0.2\ \mathrm{GeV}^{-1}<1/M_{Qq}<0.3\ \mathrm{GeV}^{-1}$). As mentioned above, we attribute this to contamination by higher momentum states, which, for large masses and volumes, are very close in energy to the zero momentum state. These points are therefore not included in the fits. Note that the term of order $1/M_{Qq}^2$ is not reliably determined in our data; it changes sign between the Wilson and the clover cases. This is not surprising since in neither case is the formalism correct through order $1/M_{Qq}^2$ for $aM_Q\sim 1$.

Using fits like those in Figs. 15–17, we now interpolate the data, replace the perturbative logarithm in Eq. (44), and divide by the appropriate $\sqrt{M_{Qq}}$ to find $f_B$, $f_{B_s}$, $f_D$, and $f_{D_s}$ for each data set. The resulting decay constants and ratios will be extrapolated to the continuum in Secs. IV and V. Before doing so, however, we repeat the analysis so far for all the other $\sim 25$ versions of reasonable plateau choices, as discussed in Sec. III C. We then find the standard deviation of the results over the other versions and add it in quadrature with the raw jackknife error of the central value. Henceforth, the statistical error of any quantity will be taken from the result of this procedure. Typically the procedure increases the statistical errors by $\sim\sqrt{2}$; we believe it mitigates any biases introduced from our choice, for the central values, of the fits with lowest statistical errors and $\chi^2_{\mathrm{cut}}$/d.o.f.

In Table VII, we collect the central values of $f_B$, $f_{B_s}$, $f_D$, and $f_{D_s}$ for the various sets. Similarly, Table VIII gives central values of ratios $f_{B_s}/f_B$, $f_{D_s}/f_D$, $f_B/f_{D_s}$, $f_{B_s}/f_{D_s}$, and $f_B/f_D$.

## IV. QUENCHED APPROXIMATION RESULTS

Final results and errors in the quenched approximation are determined much as in Ref. [4]. However, there are some significant differences, especially for the continuum extrapolation and the estimate of the associated errors. We discuss our methods in detail where they differ from [4]; where the methods are the same, we include only a very brief description for completeness.

We begin with the continuum extrapolation of various quantities. We focus on $f_B$, $f_{B_s}$, $f_{B_s}/f_B$, and $f_{D_s}$, which are probably the most important, phenomenologically. Figures 18–21 show the data for these quantities as a function of lattice spacing. The behavior of the other decay constants and ratios is similar.

It is not *a priori* obvious how to extrapolate decay constants and ratios to the continuum. As discussed in Sec. II A, our Wilson valence results have $\alpha_V^2$ errors as well as errors of the form $a\Lambda_{QCD}\times h(aM_Q)$. Here $h(aM_Q)$ is a calculable (in perturbation theory) function that is expected to be $\mathcal{O}(1)$ everywhere.[9] Since $aM_Q\gtrsim 1$ for our entire range of $a$ values, the assumption of a dominantly linear dependence on $a$ is only one possibility. A practical alternative is the assumption that, for $a$ smaller than some value, the errors are small enough that the difference with continuum values is negligible—so that extrapolation with a constant function is warranted.

We confront these assumptions with the data in Figs. 18–21. For the Wilson valence data, we show linear fits over all $a$ and constant fits for $a<0.5\ \mathrm{GeV}^{-1}$ ($\beta\geq 6.0$). Both types of fits are generally quite good. The exception is the constant fit for the ratio $f_{B_s}/f_B$. In [4], the relatively poor confidence level of the constant fit for $f_{B_s}/f_B$ (or $f_{D_s}/f_D$) relative to that of the linear fit led us to choose a linear extrapolation for the central value of the ratios. That, in turn, required choosing the linear extrapolation for the central values of the decay constants themselves, since it would be inconsistent to assume linear behavior for $f_{B_s}/f_B$ but constant behavior for $f_B$ and $f_{B_s}$ separately. Note, however, that if we just look at the two finest lattices [$a<0.36(\mathrm{GeV})^{-1}, \beta\geq 6.3$], the behavior

[9]Despite the fact that static quarks are trivially $\mathcal{O}(a)$ improved, the function $h(aM_Q)$ does not vanish even as $M_Q\to\infty$ for fixed $a$, because the Wilson light quarks still have $\mathcal{O}(a)$ errors.

TABLE VIII. Same as Table VII, but for ratios of decays constants.

| Name | $f_{B_s}/f_B$ | $f_{D_s}/f_D$ | $f_B/f_{D_s}$ | $f_{B_s}/f_{D_s}$ | $f_B/f_D$ |
|---|---|---|---|---|---|
| | | | quenched Wilson | | |
| A | 1.213(39) | 1.186(21) | 0.768(24) | 0.926(20) | 0.911(27) |
| B | 1.200(30) | 1.187(29) | 0.793(31) | 0.928(28) | 0.941(50) |
| E | 1.147(34) | 1.146(16) | 0.739(40) | 0.916(33) | 0.846(46) |
| C | 1.197(22) | 1.171(17) | 0.740(28) | 0.888(25) | 0.867(32) |
| CP | 1.191(21) | 1.152(12) | 0.752(36) | 0.899(26) | 0.867(41) |
| D | 1.142(16) | 1.124(16) | 0.755(23) | 0.866(20) | 0.849(26) |
| H | 1.145(22) | 1.128(18) | 0.776(28) | 0.888(19) | 0.875(25) |
| | | | $N_f=2$ Wilson | | |
| L | 1.168(16) | 1.162(16) | 0.777(30) | 0.918(22) | 0.903(38) |
| N | 1.162(33) | 1.173(25) | 0.788(37) | 0.927(29) | 0.924(41) |
| O | 1.160(25) | 1.137(18) | 0.789(32) | 0.916(23) | 0.897(30) |
| M | 1.191(30) | 1.159(26) | 0.793(25) | 0.928(22) | 0.920(25) |
| P | 1.168(12) | 1.172(12) | 0.784(16) | 0.914(12) | 0.919(18) |
| U | 1.196(28) | 1.162(12) | 0.763(41) | 0.904(37) | 0.886(42) |
| T | 1.134(34) | 1.131(16) | 0.840(41) | 0.958(32) | 0.950(41) |
| S | 1.158(17) | 1.146(11) | 0.790(19) | 0.927(15) | 0.905(19) |
| G | 1.179(14) | 1.158( 8) | 0.788(20) | 0.937(26) | 0.912(22) |
| R | 1.160(15) | 1.140( 8) | 0.814(28) | 0.947(20) | 0.927(32) |
| | | | quenched clover | | |
| CP1_NP-IOY | 1.156(16) | 1.120(8) | — | — | — |
| CP1_NP-tad | 1.155(16) | 1.121(9) | 0.800(19) | 0.923(12) | 0.896(18) |
| J_NP-IOY | 1.157(14) | 1.117(8) | — | — | — |
| J_NP-tad | 1.160(14) | 1.121(8) | 0.772(21) | 0.892(18) | 0.866(24) |

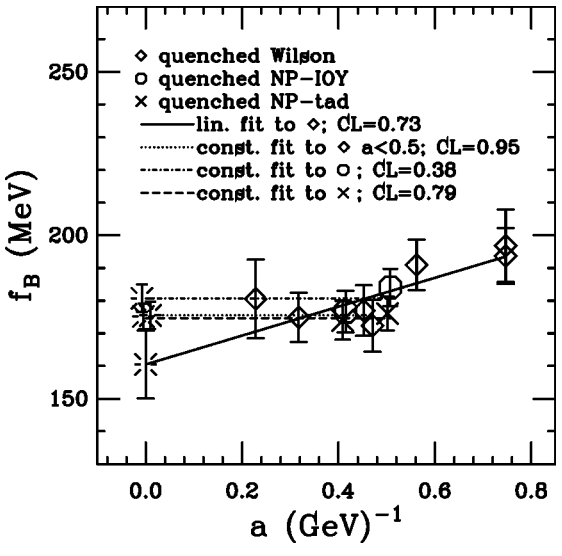


FIG. 18. $f_B$ vs $a$ for quenched lattices; the scale is set by $f_\pi$. Diamonds are results with Wilson light quarks and Wilson or static heavy quarks. Octagons and crosses are results with nonperturbative clover heavy and light quarks; ''NP-IOY'' (octagons) and ''NP-tad'' (crosses) differ in how the renormalization of the heavy quarks is performed (see text). For clarity, the octagons have been moved slightly to the right, and the fit to the crosses has been slightly lowered.

of $f_{B_s}/f_B$ is quite consistent with a constant; such a fit is also shown in Fig. 20.

The new quenched clover data, shown in Figs. 18–21 for both the NP-IOY and NP-tad schemes, have clarified the situation somewhat. The discretization errors here should be considerably smaller than for Wilson valence quarks. As discussed in Sec. II B the errors are formally $\mathcal{O}(a^2\Lambda_{QCD}^2)$ and either $\mathcal{O}(\alpha_V^2)$ (NP-IOY), or $\mathcal{O}(a^2M_Q^2)$ (NP-tad). Because there will also be a function like $h(aM_Q)$ in this case, the actual behavior with $a$ when $aM_Q\sim 1$ is likely to be complicated. The best we can do with just two clover data points is to assume that the errors are small enough that a constant extrapolation is warranted; such fits are shown in Figs. 18–21. Comparable extrapolation of clover data with a constant was performed in Refs. [17,54].

For $f_{B_s}/f_B$ the clover data show very little $a$ dependence and give a result compatible with the various constant fits to the small-$a$ Wilson data. The clover results are not compatible with the linear extrapolation of the Wilson data, which are now seen to give a rather low result. Recent preliminary quenched results [45] with clover valence quarks on Symanzik improved glue are also incompatible with the Wilson linear extrapolation. For our central quenched value of $f_{B_s}/f_B$ or $f_{D_s}/f_D$ we therefore drop the linear Wilson extrapolation and average the four constant extrapolations: two for Wilson ($a<0.5$ GeV$^{-1}$ and $a<0.36$ GeV$^{-1}$) and two

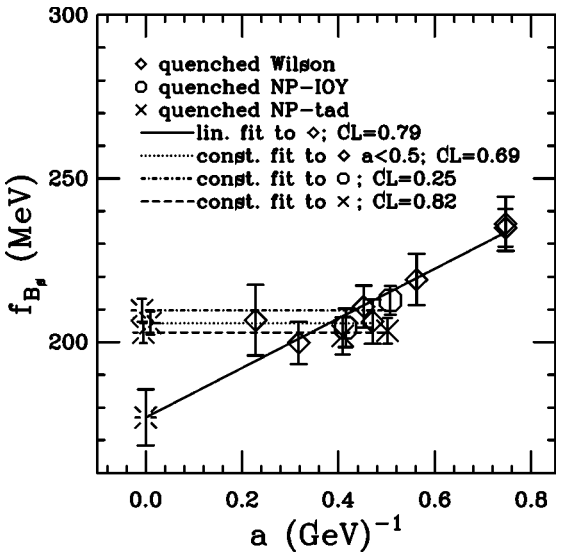


FIG. 19. Same as Fig. 18, but for $f_{B_s}$. For clarity, the octagons have been moved slightly to the right.

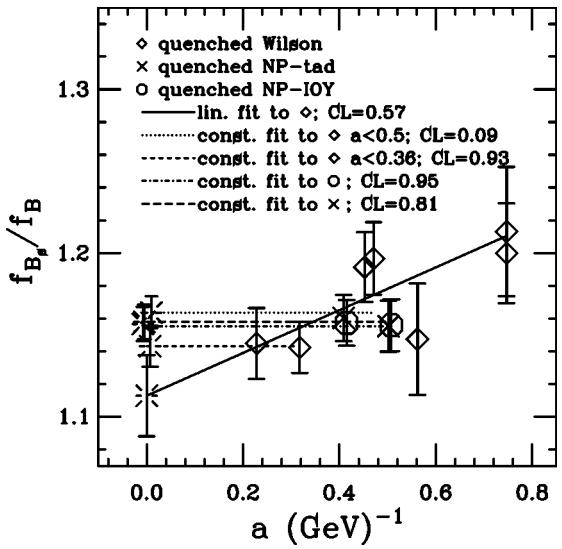


FIG. 20. $f_{B_s}/f_B$ vs $a$ for quenched lattices. Labels are the same as in Fig. 18, but one additional fit is shown: a constant fit to the two diamonds (Wilson quark results) with smallest $a$ ($a < 0.36$ GeV$^{-1}$). For clarity, the octagons have been moved slightly to the right and the fit to the octagons has been slightly lowered.

for clover (NP-IOY and NP-tad).[10] The systematic error of the continuum extrapolation is then taken as the standard deviation of the four individual extrapolations. The other decay constant ratios ($f_B/f_{D_s}$, $f_{B_s}/f_{D_s}$, and $f_B/f_D$) are treated similarly, although there is one fewer result to average, since NP-IOY is not applicable.

Though we have dropped the linear extrapolation from the analysis of the ratios, it is not inconsistent to include it in the analysis of the decay constants themselves. Indeed, for $f_B$ and $f_{B_s}$, the downward trend of the clover data as $a$ decreases makes it difficult to rule out the linear extrapolation of the Wilson data. On the other hand, constant clover extrapolations do give results closer to the constant Wilson extrapolations than to the linear Wilson extrapolations. For $f_{D_s}$ (and $f_D$, not shown), the situation is reversed: The clover data have an upward trend as $a$ decreases; yet constant clover extrapolations give results (slightly) closer to the linear Wilson extrapolations than to the constant Wilson extrapolations. To obtain the central values of the decay constants, we therefore average the results of all the extrapolations and take the standard deviation of the results as the continuum extrapolation error. For $f_B$ and $f_{B_s}$ a total of four fits are included: linear Wilson, constant Wilson, constant NP-IOY and constant NP-tad. For $f_D$ and $f_{D_s}$ there are three fits, since NP-IOY is omitted.

As described in Sec. III D, we estimate the chiral extrapolation errors by comparing (after continuum extrapolation) the central values (which use ''chiral choice I'') with those obtained by changing the chiral fits of the heavy-light and light-light decay constants from linear to quadratic (''chiral choice II'').[11] The errors of the chiral extrapolation and other systematic errors within the quenched approximation are collected in Tables IX and X. Note that the quoted chiral errors are all positive. This can be traced to the effect of the quadratic extrapolation of $f_{qq}$ (used to set the scale through $f_\pi$), which is clearly, though slightly, concave down (see Figs. 6 and 7). The concavity in $f_{Qq}$ in the region of the $B$ is less pronounced.

The perturbative error is estimated by varying, over a ''reasonable range,'' the values of $q^*$ used in the one-loop renormalization constants. For Wilson fermions, we take the range for the heavy-light currents to be $1/a \leqslant q^* \leqslant 2.86/a$, with $1.43/a$ the central value, as described in Sec. II A. Similarly, for the light-light Wilson currents $q^*$ ranges between $1/a$ and $4.63/a$, with $2.32/a$ the central value. In the clover case, perturbation theory for the heavy-light currents is only relevant for NP-IOY. For central values, we take $q^* = 3.34/a$ (set CP1) and $q^* = 2.85/a$ (set J), which come from the static-light calculation of [11] with the corresponding clover coefficients. The scale $q^*$ is then allowed to range between $1/a$ and twice the central value. For light-light clover currents, only $b_A$ is treated perturbatively; the central value for $q^*$ is taken to be $1/a$ (see Sec. II B). This gives the central values for $b_A$ shown in Table II. The upper end of the range of $b_A$ shown comes from taking $q^* = 0.7/a$; the lower end, from using ''boosted perturbation theory'' with $g^2$

[10]Although the calculation in Ref. [28] is not well controlled at the $D$ mass, the NP-IOY procedure may be used for $f_{D_s}/f_D$ because the renormalizations cancel. Note that NP-tad involves the light quark mass in the renormalizations [see Eqs. (16) and (19)] so does not give identical results to NP-IOY even for $f_{B_s}/f_B$ or $f_{D_s}/f_D$.

[11]In the dynamical case, we attempt to estimate an additional chiral error coming from chiral logarithms by performing a separate chiral extrapolation of $f_{qq}/f_{Qq}$. (See Secs. III E and V D.) This is not feasible in the quenched case: the quenched chiral logs in $f_{Qq}$ have coefficients with unknown magnitude and sign [55]; while $f_{qq}$ has no quenched logs at all at one loop [56].

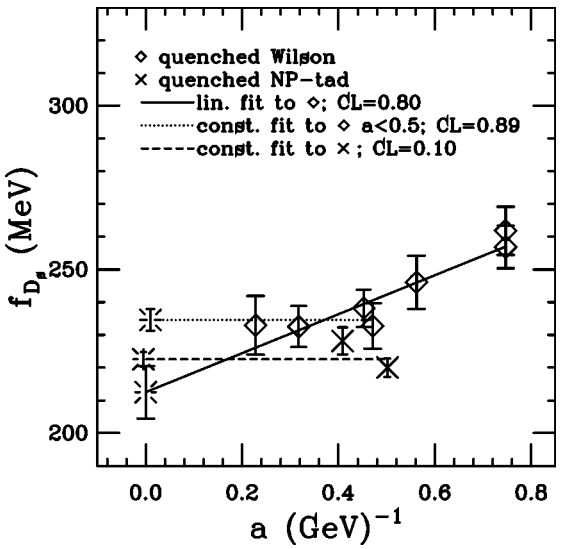


FIG. 21. $f_{D_s}$ vs $a$ for quenched lattices. Labels are the same as in Fig. 18, but the NP-IOY points have been omitted because the perturbative calculation is not available at the relevant lattice masses.

$=6/(\beta\langle P\rangle)$ ($\langle P\rangle$ is the mean plaquette, normalized to have maximum 1). This is equivalent to taking a $q^*$ of roughly $5.25/a$, so we are using a rather conservative range.

As mentioned in Sec. II A, there is a systematic error associated with the fact that $c_{mag}\equiv M_2/M_3$ is not equal to 1 with Wilson fermions. Because $c_{mag}$ has a complicated dependence on $a$, this error is not removed by any of the simple extrapolations available to us. One may argue that the residual effect is just one particular discretization error and therefore has already been included. However, if one models this error for both linear and constant extrapolations using Eq. (4) for $M_2$ and $M_3$ (along the lines of what was done in Refs. [17] and [4]), one finds that the error is larger with a constant extrapolation but has the same (but unknown) sign in both cases. Therefore we believe it reasonable to include as an additional error the linear extrapolation estimate of the Wilson magnetic mass error. From the tadpole improved tree-level model, one estimates these errors as $\sim 2\%$ for $f_B$ and $\sim 3\%$ for $f_D$ (see [4]). An alternative estimate comes from the comparison of the results of interpolations to the physical heavy meson masses using the ''heavier-heavies'' [fit (i)—see Sec. III F] with those using the ''lighter-heavies'' [fit (ii)]: the lighter masses are affected much less by the magnetic mass error, and the static point is not affected at all. We take the larger of the two estimates as our magnetic mass error for Wilson fermions.

The magnetic mass error is absent for clover fermions. Therefore, in our final error budgets (Tables IX and X) we multiply the Wilson magnetic mass error by 1/2 or 2/3, depending on the relative number of Wilson and clover estimates that go into the central value.

Note that the magnetic mass errors in the tables are considerably smaller for $B$ mesons than for $D$ mesons, despite the fact that the difference between $M_2$ and $M_3$ increases with the lattice mass. The point is that the magnetic mass errors are systematic effects on the $1/M_Q$ corrections, and such corrections are inherently bigger for $D$ mesons than for $B$'s. Further, especially large errors can be introduced if $1/M_Q$ fits in the range of the $B$ are extrapolated back to the $D$ region. For that reason we always use fit (ii) (''lighter-heavies'') for central values of ratios that involve both $D$'s and $B$'s: $f_B/f_{D_s}$, $f_{B_s}/f_{D_s}$, and $f_B/f_D$.

The remaining two systematic errors, the effect of the interpolation in $1/M_{Qq}$ and the finite size errors, are estimated just as in Ref. [4]. For the central values, we truncate the fit of $f_{Qq}\sqrt{M_{Qq}}$ vs $1/M_{Qq}$ at quadratic order. We estimate the error thereby introduced by changing to cubic fits (with mass range 1.25 to 4 GeV, plus the static point when available). The errors found are $\sim 1\%$; this is what one would expect if the mass scale of the cubic term is $\sim 0.75$ GeV, roughly the scale size found in the linear and quadratic terms.

We estimate the finite volume effects by finding the fractional difference between results on set A (spatial size $\sim 1.2$ fm) and set B ($\sim 2.5$ fm). Since set A is smaller than

TABLE IX. Central values ($f_\pi$ scale) and errors in MeV for the quenched decay constants. The statistical errors and the effects of excited states are combined, as described at the end of Sec. III F. Errors marked with explicit + or − signs are treated as signed; all others are treated as symmetric. The scale and $\kappa_s$ errors are not included in the total error *within* the quenched approximation but are shown for completeness.

| | $f_B$ | $f_{B_s}$ | $f_D$ | $f_{D_s}$ |
|---|---|---|---|---|
| Central value | 173.0 | 198.8 | 199.5 | 223.2 |
| | | errors | | |
| Statistics and excited states | 5.7 | 4.7 | 5.6 | 4.6 |
| Continuum extrapolation | 8.7 | 14.8 | 4.9 | 11.1 |
| Chiral extrapolation | +8.6 | +9.4 | +4.3 | +6.5 |
| Perturbative | 9.6 | 14.1 | 6.6 | 10.9 |
| Magnetic mass | 1.7 | 1.9 | 5.1 | 5.7 |
| $1/M$ fit | 2.0 | 1.7 | 0.5 | 0.2 |
| Finite volume | +2.8 −8.5 | +1.0 −7.8 | +3.8 −5.1 | +4.3 −4.1 |
| Scale (change to $m_\rho$) | −3.5 | −5.9 | +4.2 | +4.0 |
| $\kappa_s$ (change to $\phi$) | — | +3.7 | — | +2.3 |

TABLE X. Same as Table IX but for decay constant ratios.

| | $f_{B_s}/f_B$ | $f_{D_s}/f_D$ | $f_B/f_{D_s}$ | $f_{B_s}/f_{D_s}$ | $f_B/f_D$ |
|---|---|---|---|---|---|
| Central value | 1.155 | 1.128 | 0.769 | 0.891 | 0.871 |
| | | | errors | | |
| Statistics and excited states | 0.011 | 0.008 | 0.015 | 0.012 | 0.016 |
| Continuum extrapolation | 0.009 | 0.012 | 0.017 | 0.019 | 0.013 |
| Chiral extrapolation | $+0.003$ | $+0.014$ | $+0.009$ | $+0.009$ | $+0.020$ |
| Perturbative | 0.008 | 0.011 | 0.015 | 0.020 | 0.017 |
| Magnetic mass | 0.000 | 0.000 | 0.015 | 0.018 | 0.017 |
| $1/M$ fit | 0.001 | 0.000 | 0.006 | 0.008 | 0.009 |
| Finite volume | $+0.012\ -0.013$ | $+0.008\ -0.000$ | $+0.025\ -0.000$ | $+0.003\ -0.009$ | $+0.028\ -0.000$ |
| Scale (change to $m_\rho$) | $+0.001$ | $-0.001$ | $+0.009$ | $+0.008$ | $+0.007$ |
| $\kappa_s$ (change to $\phi$) | $+0.025$ | $+0.018$ | $-0.009$ | $+0.004$ | — |

the other quenched lattices ($\sim$1.3–1.5 fm) and B is much larger, this should bound the finite volume error. To be conservative, we consider both: (a) the difference when all quantities are computed individually on sets A and B and (b) the difference when the light-light quantities are held fixed to their values from set 5.7-large. Since $f_\pi$ generally suffers larger finite size effects than $f_{Qq}$, these two estimates typically have opposite signs; in that case we include both estimates as signed errors. When the estimates have the same sign, however, we simply choose the larger.

Tables IX and X also show errors associated with fixing the scale (changing from $f_\pi$ to $m_\rho$) and fixing $\kappa_s$ (changing from using the pseudoscalars to using the $\phi$ meson). Logically, these should be considered errors *of* the quenched approximation, not *within* the quenched approximation, and are not included in this section. Indeed, the question ''what is $f_B$ in the quenched approximation?'' is only well defined when one specifies how the scale is fixed. Even in the continuum limit, different scale choices (and different ways of fixing $\kappa_s$ for strange-quark quantities) must give different results in the quenched approximation. The differences should of course go away in the continuum limit of the full theory. In Sec. V, where we attempt to quote results that can be directly compared with experiment, such errors are taken into account.

Our final results for heavy-light decay constants *within* the quenched approximation (fixing the scale by $f_\pi$) are

$$f_B = 173(6)(16)\ \text{MeV}; \quad f_{B_s} = 199(5)(^{+23}_{-22})\ \text{MeV}$$

$$f_D = 200(6)(11)\ \text{MeV}; \quad f_{D_s} = 223(5)(^{+18}_{-17})\ \text{MeV}$$

$$\frac{f_{B_s}}{f_B} = 1.16(1)(2); \quad \frac{f_{D_s}}{f_D} = 1.13(1)(2)$$

$$\frac{f_B}{f_{D_s}} = 0.77(2)(^{+4}_{-3}); \quad \frac{f_{B_s}}{f_{D_s}} = 0.89(1)(^{+4}_{-3})$$

$$\frac{f_B}{f_D} = 0.87(2)(^{+5}_{-3}). \tag{45}$$

The errors are statistical and systematic (within the quenched approximation), respectively. Relevant systematic errors in Tables IX and X have been combined in quadrature. Errors whose signs are not likely to be reliably determined by our procedures (continuum extrapolation, perturbation theory, magnetic mass, $1/M$ fits) have been treated as symmetric errors. The others (chiral extrapolation and finite volume) have been treated as signed errors. The results in Eq. (45) differ from those in Ref. [4] due to (i) inclusion of new data from sets CP, CP1 and J; (ii) setting the central value of the heavy-light scale from the static-light calculation of Ref. [11], rather than that of Ref. [22]; and (iii) other changes in analysis, motivated by the new runs. The most important of these is the way we find the central value of the continuum extrapolation (as discussed above, we now average our four possible versions rather than taking only the linear Wilson fit). In addition, the details of the error estimate for the chiral extrapolation have changed. Some alternative chiral fits used previously—e.g., linear fits of $m_\pi^2$ vs quark mass—are convincingly excluded by the new data.

## V. RESULTS WITH DYNAMICAL QUARKS

### A. Continuum extrapolation

Dynamical $N_f=2$ results for $f_B$, $f_{B_s}$, $f_{B_s}/f_B$, and $f_{D_s}$ as a function of lattice spacing are shown in Figs. 22, 23, 24, and 25, respectively. Leaving aside the ''fat clover'' results for now, the data in all cases seem to favor constant fits; indeed, the best linear fits have very small slopes. Note however that the smallest lattice spacing here is $\sim 0.45\ (\text{GeV})^{-1} \approx 0.09$ fm; whereas in the quenched case we have data down to $\sim 0.23(\text{GeV})^{-1} \approx 0.045$ fm. It is thus possible that the apparent independence of lattice spacing is due to the cancellation of two effects: (i) an overall decrease as lattice spacing decreases, which was one of the alternatives considered in the quenched case, and (ii) the turning on of short distance dynamical fermion effects as one moves away from the quite coarse spacings of sets L and N. The latter effect could be exacerbated by staggered flavor violations, which would be especially large on the coarsest lattices and which would reduce the effective number of dynamical flavors.

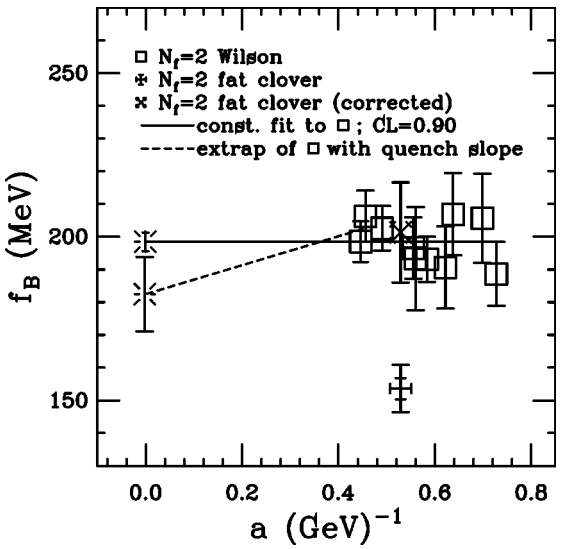


FIG. 22. $f_B$ vs $a$ for dynamical $N_f=2$ lattices; a few points have been moved a slight distance horizontally for clarity. Squares are results with light Wilson valence quarks and Wilson or static heavy valence quarks. From left to right, the squares come from $\beta=5.6$ (sets G, R, S, T, U), $\beta=5.5$ (sets P, M, O, N), and $\beta=5.445$ (set L). The solid line is a fit of all the Wilson results to a constant. The dashed line shows what would happen if the dynamical results decreased for smaller lattice spacing with the same slope as the linear fit to the corresponding quenched data. The fancy plus is the result with fat-link clover valence quarks (light and heavy) on set RF. The fancy cross shows the ''corrected'' value (see text). The fat clover data (corrected or uncorrected) are not included in our final results.

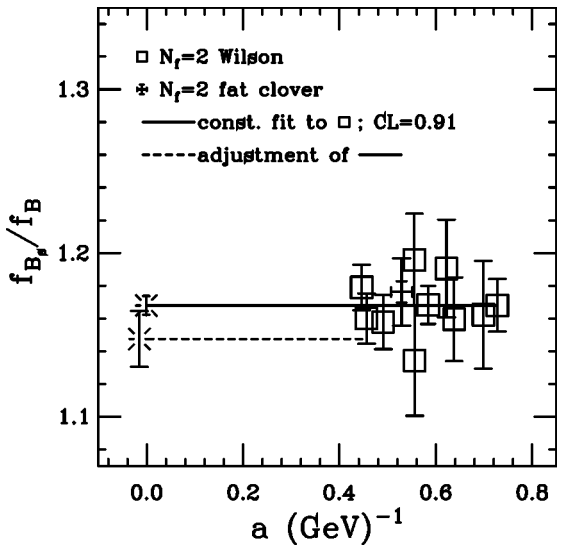


FIG. 24. $f_{B_s}/f_B$ vs $a$ for dynamical $N_f=2$ lattices. Labels are the same as in Fig. 22, but no correction to the fat-link clover result is needed for the ratio of decay constants. The alternative dashed line assumes a drop when $a\to 0$ that is the same as the difference in the quenched case between a constant fit to the results from the highest three $\beta$ values and a constant fit to those from the highest two $\beta$ values.

If the above possibility is realized, then the $N_f=2$ results could well begin to decrease for still smaller lattice spacings as the quenched-like behavior sets in. For the decay constants, we therefore consider two alternative extrapolations: the constant extrapolation of all $N_f=2$ data, and a linear extrapolation that begins at the average value of the results on the two finest lattices (sets R and G) and then continues to the continuum limit with the quenched slope (see Figs. 22, 23, and 25). For ratios of decay constants, we ruled out the linear extrapolation in the quenched case. Yet the two finest quenched lattices (D and H) have in general lower values for the ratios than the averages that include the quenched sets (C and CP) that are comparable to the finest $N_f=2$ lattices. The two alternatives for ratios are therefore taken to be (i) the constant extrapolation of all $N_f=2$ data, and (ii) the first extrapolation reduced by the quenched difference: (average of C, CP, D, and H) $-$ (average of D and H). Figure 24 shows these alternatives. In all cases we then take the central value to be the average of the two alternatives, and the error

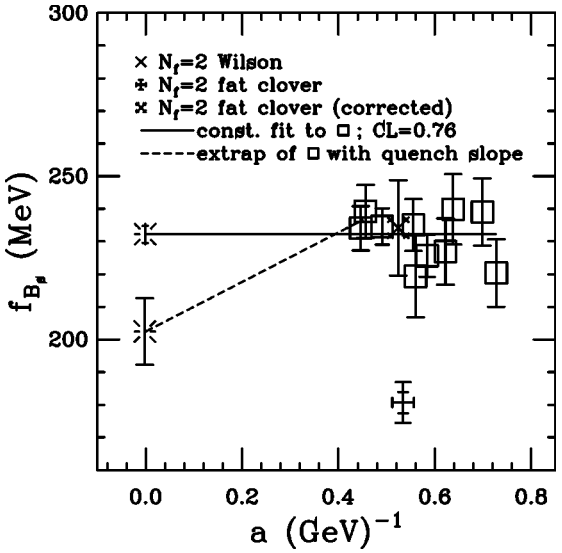


FIG. 23. Same as Fig. 22, but for $f_{B_s}$.

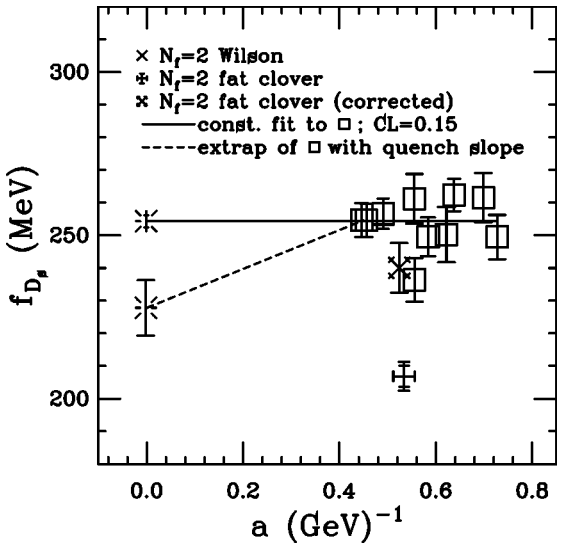


FIG. 25. Same as Fig. 22, but for $f_{D_s}$.

TABLE XI. Central values ($f_\pi$ scale) and errors in MeV for the dynamical ($N_f=2$) decay constants. As in Tables IX and X, the statistical errors and the effects of excited states are combined. The errors above the line (i.e., up to and including finite volume errors) are treated as errors within the $N_f=2$ partially quenched approximation. Errors below the line are treated as errors of that approximation. In general, errors marked with explicit + or − signs are treated as signed, and other errors are treated as symmetric. The exception is partial quenching, where we do not take the sign seriously but show it nevertheless in parentheses.

| | $f_B$ | $f_{B_s}$ | $f_D$ | $f_{D_s}$ |
|---|---|---|---|---|
| Central value | 190.5 | 217.3 | 214.9 | 241.0 |
| | | errors | | |
| Statistics and excited states | 7.1 | 6.4 | 6.1 | 5.2 |
| Continuum extrapolation | 11.3 | 21.0 | 8.5 | 18.7 |
| Valence chiral extrapolation | +16.6 | +14.7 | +7.5 | +8.3 |
| Perturbative | 12.0 | 18.5 | 8.2 | 15.1 |
| Magnetic mass | 3.8 | 4.4 | 8.4 | 9.7 |
| $1/M$ fit | 2.6 | 2.7 | 1.0 | 0.9 |
| Finite volume | +7.7→0.0 | +5.2→0.0 | +3.4→0.0 | −0.1→0.0 |
| Partial quenching | (+)2.4 | (−)3.0 | (+)3.4 | (−)3.8 |
| Scale (change to $m_\rho$) | +10.6 | +8.7 | +5.4 | +3.9 |
| $\kappa_s$ (change to $\phi$) | — | +3.9 | — | +2.3 |
| Missing dynamical $s$ quark | +8.7 | +9.2 | +7.7 | +8.9 |

of the continuum extrapolation to be the ''sample standard deviation'' of the two (dividing by $n-1=1$, not $n=2$). Central values and errors for the $N_f=2$ data are shown in Tables XI and XII.

### B. Fat links

In the above discussion of the continuum extrapolation, we ignored the fat-link clover results. If taken at face value, these results would imply the existence of extremely large discretization errors. We therefore need to examine the fat-link computations in detail. These computations use valence quarks—both heavy and light—with the standard clover action, but with gauge links that have first been ''fattened'' by $N$ iterations of APE smearing [57]. The coefficient of the sum of the staples is $c/6$ and that of the forward link is $1-c$; a projection back into $SU(3)$ is included after each smearing step. The fat-link results (set RF) displayed in Figs. 22–25 have $N=10$, $c=0.45$. The clover coefficient $c_{\rm SW}$ is taken to have its tree-level value (1.0); this is also approximately the tadpole-improved value, since the fattening strongly suppresses tadpole contributions. Physically, APE smearing corresponds roughly to a Gaussian smearing of the fermion-gauge field interaction over a range $\langle x^2\rangle \simeq cN/3$ [58].

Various kinds of fat links have come to play a major role in lattice simulations in the last few years. The motivation for introducing them in the context of Wilson-like fermions [59] was that they improve the chiral properties of the fermions. This happens in several (related) ways: First, fat links reduce additive mass renormalization. They also suppress exceptional configurations, which present a severe challenge to clover computations on our dynamical lattices [12,60]. (This

TABLE XII. Same as Table XI but for decay constant ratios.

| | $f_{B_s}/f_B$ | $f_{D_s}/f_D$ | $f_B/f_{D_s}$ | $f_{B_s}/f_{D_s}$ | $f_B/f_D$ |
|---|---|---|---|---|---|
| Central value | 1.158 | 1.142 | 0.793 | 0.922 | 0.913 |
| | | | errors | | |
| Statistics and excited states | 0.011 | 0.009 | 0.016 | 0.013 | 0.016 |
| Continuum extrapolation | 0.015 | 0.014 | 0.005 | 0.004 | 0.001 |
| Valence chiral extrapolation | −0.016 | +0.005 | +0.032 | +0.019 | +0.037 |
| Perturbative | 0.012 | 0.011 | 0.034 | 0.043 | 0.042 |
| Magnetic mass | 0.003 | 0.002 | 0.024 | 0.028 | 0.027 |
| $1/M$ fit | 0.001 | 0.000 | 0.014 | 0.020 | 0.015 |
| Finite volume | −0.019→0.000 | −0.018 | +0.026→0.000 | +0.010→0.000 | +0.016→0.000 |
| Partial quenching | (−)0.023 | (−)0.026 | (+)0.027 | (−)0.021 | (+)0.008 |
| Scale (change to $m_\rho$) | −0.010 | −0.005 | +0.015 | +0.017 | +0.015 |
| $\kappa_s$ (change to $\phi$) | +0.014 | +0.017 | −0.008 | +0.004 | — |
| Missing dynamical $s$ quark | +0.001 | +0.007 | +0.012 | +0.015 | +0.021 |

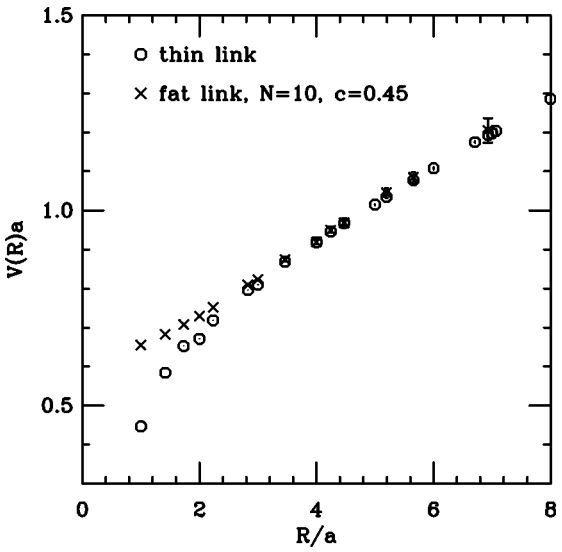


FIG. 26. Static potential at quenched $\beta=5.85$ with and without $c=0.45$, $N=10$ APE-smeared fattening.

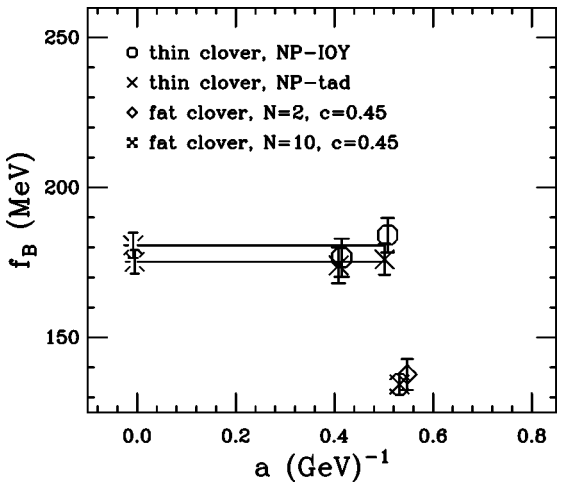


FIG. 27. Effect of smearing on quenched $f_B$. The thin clover points are at $\beta=6.0$ and 6.15 (sets CP1 and J); the fat, at $\beta=6.0$ (set CPF). The extrapolation of the thin clover results to the continuum is also shown.

occurs because they shrink the range of the real eigenmodes of the Dirac operator.) Finally, in perturbation theory, fat links bring the vector and axial vector renormalization constants $Z_V$ and $Z_A$ (as well as the scalar and pseudoscalar renormalization constants) closer together.

Simulations of light quark systems with a variety of fat link actions at lattice spacings in the range 0.1–0.2 fm show little dependence of physical observables on the amount of fattening, even for the very aggressive amount of fattening of the simulations we report here. For many quantities, this amount of fattening also gives quite small discretization errors [61].

We take the light-light renormalization coefficients for fat-link clover fermions from the perturbative calculations of Ref. [11]. The heavy-lights (for which perturbative calculations do not exist) are normalized using the *static-light* results of [11]. Although one expects that this should be roughly correct for the large values of $aM$ at the $B$ meson, it introduces a possibly serious source of systematic error into the fat-link results.

As first reported in Ref. [12], the fat-link clover results for decay constants are seen to be much smaller than the apparent continuum-limit results of the Wilson quarks. Simulations of $\overline{Q}Q$ systems with fat-link quarks also show that fattening suppresses the magnitude of vector-pseudoscalar mass splitting. A measurement of the heavy quark potential gives some qualitative understanding of both effects: the attractive short distance piece of the potential is washed away by the fattening. This is shown in Fig. 26, where we compute the static potential using $c=0.45$, $N=10$ APE-smeared fat links at quenched $\beta=5.85$. The loss of this part of the potential leads to a suppression of the heavy quark wave function at the origin. Although this is an effect that would vanish in the continuum limit (for fixed $N$, $c$), it could introduce large scaling violations for short-distance-sensitive quantities.

To study more directly the effect of fattening on heavy-light decay constants, we have computed the decay constants with clover fermions on a 99 lattice subset of quenched set CP1, which we call CPF. We have tried four different levels of fattening: $c=0.45$ with $N=2$, 6, and 10, and $c=0.25$ with $N=7$. In these cases, $c_{\rm SW}$ is set equal to the tadpole-improved tree level value $1/u_0^3$, with $u_0$ determined by the plaquette computed with the smeared links. The renormalization constants are determined in the same way as for the dynamical case (set RF). A comparison of two of the smearing levels with the thin-link clover computations is shown in Fig. 27. The fat-link $f_B$ values are considerably suppressed compared to those from the thin links, which in turn are consistent with the results of continuum-extrapolated quenched Wilson fermions (see Sec. IV).

Figure 27 shows that the suppression produced by the lowest and highest levels of fattening are consistent. In fact, there is not much difference in the values of the heavy-light decay constants among the four different levels of fattening we studied, even though the amount of smoothing introduced into the short-distance potential is quite different for the four cases. Furthermore, the light-light decay constants with fat clover and thin clover links differ by only $\sim 7\%$: Compare the $f_\pi$-determined lattice spacings of sets CP1 and CPF in Fig. 27, or see Table V. Note that in the light-light case we are using the correct renormalization factors from Ref. [11]. This suggests that the $\sim 25\%$ suppression of heavy-light decay constants for our fat links may be due more to the use of the incorrect renormalizations (static-light instead of heavy-light) than to scaling violations from the smoothing of the short-distance potential. Be that as it may, these quenched studies show that the fat clover $N_f=2$ results may be ignored, at least until fat-link heavy-light renormalization constants are available.

An alternative approach would be to try to correct the fat-link clover dynamical results by the factor (thin link quenched)/(fat link quenched) at a comparable lattice spacing. We can do this since the lattice spacings for sets CPF

(quenched) and RF ($N_f=2$) are quite close. (See Table V.) The corrected fat-link results shown in Figs. 22, 23, and 25 are consistent with the Wilson $N_f=2$ results. However, we judge that the reasons for the fat-link suppression are not well enough understood to be confident that the correction factor is the same in the quenched and dynamical cases. We therefore drop the fat clover $N_f=2$ results and use the Wilson results only.

We emphasize that fat-link actions are formally neither better nor worse than actions with thin links—the differences lie only in the composition and strength of higher dimensional (irrelevant) operators. However, from a practical point of view one is interested in actions for which particular quantities scale well with lattice spacing. Fat links are intended to improve chirality, but chirality is a property of light quarks, not heavy ones. In hindsight, there is no physical motivation to construct or use fat-link actions for heavy quarks. Some recent developments [62] for fat-link actions for light quarks have been influenced by our negative experience—one of the design criteria is to minimize effects such as are shown in Fig. 26. We are currently studying the behavior of decay constants simulated with thin-link heavy quarks and fat-link light quarks.

### C. Partial quenching and chiral extrapolation

Our central values with $N_f=2$ are computed in the ''partially quenched'' approximation: dynamical quark configurations are treated as fixed backgrounds and chiral extrapolation is performed in the valence quark mass only. The main justification for using the partially quenched approximation can be seen qualitatively in Figs. 22–25: For our range of dynamical quark masses and with our statistical and systematic errors, there is no obvious trend in the decay constants when the dynamical quark mass is varied at fixed $\beta$. (This statement is examined in more detail below.)

The standard systematic error associated with the valence-mass chiral extrapolation is then estimated in exactly the same way as in the quenched approximation (comparison of ''chiral choice I'' with ''chiral choice II'' — see Secs. III D and IV). Effects of chiral logarithms at very low quark mass are considered separately in Sec. V D.

To estimate the systematic error due to partial quenching, we perform a complete additional analysis in the ''fully unquenched'' theory, where the light $(u,d)$ valence quark mass on a given lattice set is interpolated or extrapolated to the value of the dynamical mass on that set. Since the valence and dynamical quarks are simulated with different lattice actions, the equality must be defined by some physical quantity. We demand that the pseudoscalar (''pion'') have the same mass with either action. We then perform chiral extrapolations of $f_{Qq}$ with $m_{q,\mathrm{valence}}=m_{q,\mathrm{dynamical}}$ using data from sets at fixed $\beta$: either $\beta=5.6$ (sets G, R, S, T, U) or $\beta=5.5$ (sets P, M, O, N). Such extrapolations must be performed in physical units because they involve different sets with different lattice spacings. To set the scale, we use as usual $f_{qq}$, extrapolated in valence quark mass to the physical $u,d$ point, i.e., $f_\pi$. Note that the scale is set in a partially quenched manner. However the fully unquenched theory is recaptured once the dynamical mass is itself extrapolated to the physical $u,d$ point.[12]

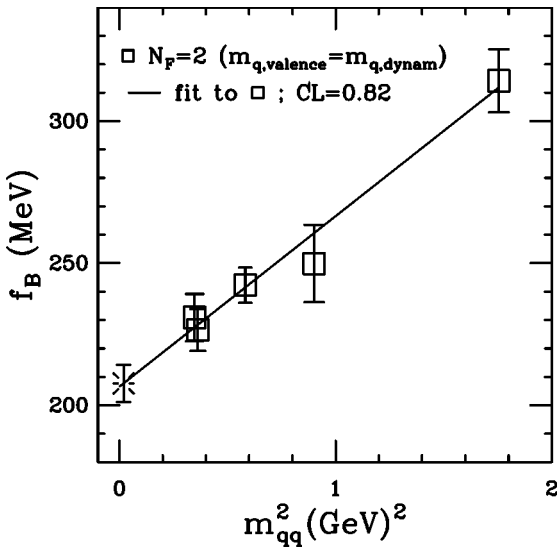


FIG. 28. ''Fully unquenched'' chiral extrapolation of $f_B$ at $\beta=5.6$ (sets G, R, S, T, U). The burst shows the extrapolated value when $m_{qq}^2=m_\pi^2$.

In Fig. 28 we show the chiral extrapolation of $f_B$ with $m_{q,\mathrm{valence}}=m_{q,\mathrm{dynamical}}$ at $\beta=5.6$. We call the dependent variable ''$f_B$'' because the heavy quark has already been interpolated to the $b$ quark mass, as in Sec. III F. As an independent variable, we use the pseudoscalar mass squared, $m_{qq}^2$, and extrapolate to $m_{qq}^2=m_\pi^2$. Note that the linear fit is excellent, even though it includes very heavy $m_{qq}$ values. However, if we restricted $m_{qq}$ to a safer range for a chiral extrapolation $[m_{qq}^2<0.6\ (\mathrm{GeV})^2]$, the results would be essentially unchanged. The behavior of $f_D$ is very similar to that of $f_B$.

Figure 29 shows $f_{B_s}$ as a function of the dynamical quark mass at $\beta=5.6$. The light valence quark mass has already been interpolated to the strange quark mass, and only the dynamical $u,d$ quark mass is varied. With the current statistical and discretization errors, there is little evidence here for dynamical quark mass dependence (using an $f_\pi$ scale). This may be due, at least partially, to staggered flavor violations, which reduce the effective range over which the dynamical mass varies. Note, however, that there *is* a significant difference when one compares these dynamical mass points to the infinite mass case (the quenched approximation): compare Figs. 19 and 23. The behavior of $f_{D_s}$ is nearly identical to that seen in Fig. 29; the other decay constants, such as $f_B$, have similar behavior when they are plotted as a function of

[12]This approach could be dangerous if the dependence of $f_{qq}$ on the dynamical quark mass at fixed valence mass were so violent that the chiral extrapolation of $f_{Qq}$ in physical units became uncontrolled. This does not appear to be the case, as seen in Figs. 28–30 below. However, in a work in progress [45], we employ a safer approach, in which the dynamical lattices have matched scales set independently of the valence quarks using the static quark potential.

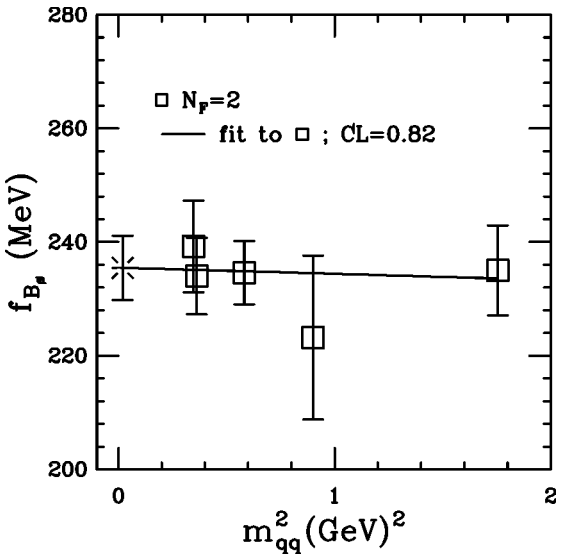


FIG. 29. Same as Fig. 28 but for $f_{B_s}$. The valence quark masses do not vary but are held fixed at the masses of the *b* and *s*. The fit is linear (not a constant), but has quite small slope.

the dynamical mass for fixed valence mass.

The chiral extrapolation of $f_{D_s}/f_D$ as a function of dynamical quark mass (represented by the dynamical $m_{qq}^2$) is shown in Fig. 30. For $f_D$, the light valence quark mass is put equal to the dynamical mass; while for $f_{D_s}$, it is kept equal to the physical strange mass. Since $f_{D_s}$ has fixed valence quark mass, it, like $f_{B_s}$, changes little with dynamical quark mass; while $f_D$ varies more or less linearly, like $f_B$. We therefore fit $f_{D_s}/f_D$ to the inverse of a linear function in $m_{qq}^2$, i.e., to $1/(c+dm_{qq}^2)$, with *c* and *d* allowed to vary. The ratio $f_{B_s}/f_B$ is fit in the same way; while the ratios $f_B/f_{D_s}$, $f_{B_s}/f_{D_s}$, and $f_B/f_D$ are fit to linear functions. (The latter two ratios are,

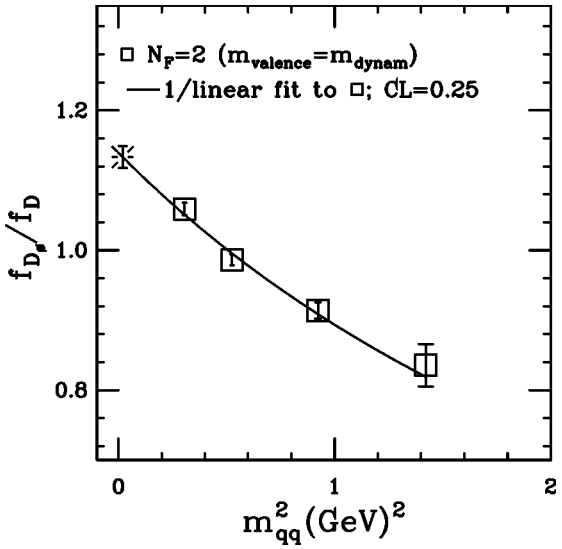


FIG. 30. Chiral extrapolation of $f_{D_s}/f_D$ at $\beta=5.5$ (sets P, M, O, N) with the light valence quark mass in $f_D$ equal to the dynamical quark mass. The quantity $1/(f_{D_s}/f_D)$ is fit to a linear function.

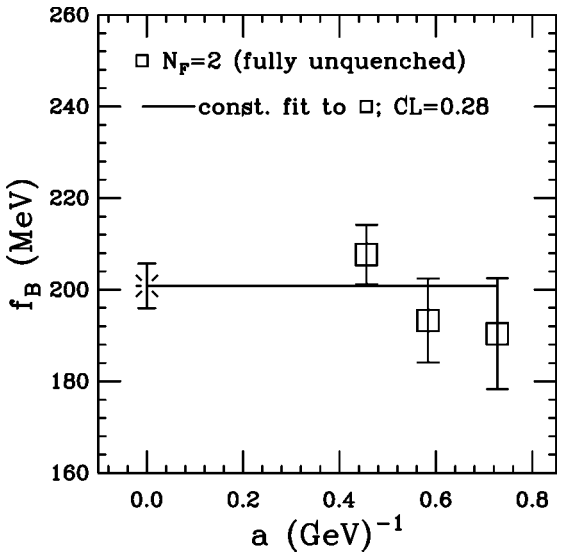


FIG. 31. Lattice spacing dependence of $f_B$ after fully unquenched chiral extrapolation. From left to right, the points represent: $\beta=5.6$, 5.5, and 5.445. When there is more than one lattice spacing at a given $\beta$, the points are plotted at the lattice spacing of the finest lattice (lowest dynamical mass). Thus $\beta=5.6$ and 5.5 are represented by the lattice spacing of sets R and P, respectively. The fit is to a constant.

like $f_{B_s}$, almost independent of the dynamical quark mass, and so the fitting form makes little difference as long as constant behavior is allowed.)

We can now examine the dependence of the fully unquenched quantities on lattice spacing. Unfortunately, we can perform the fully unquenched analysis only at two $\beta$ values, 5.5 and 5.6, for each of which lattice sets exist with four different dynamical quark masses. At the third $\beta$ value of our dynamical simulations ($\beta=5.445$), we have only a single dynamical mass ($am=.025$, set L). We attempt a chiral extrapolation there by using the average of the (physical) parameters describing the $m_{qq}^2$ dependence at $\beta=5.6$ and 5.5 (as determined above). Each parameter has a statistical error estimated by propagating the statistical errors of the $\beta=5.6$ and 5.5 data, and a systematic error taken to be the difference between the average value and the $\beta=5.5$ value. The overall error at $\beta=5.445$ is then determined by adding in quadrature the intrinsic statistical error from set L and the statistical and systematic errors coming from the chiral extrapolation. The amount of chiral extrapolation required for set L is actually quite small because the physical dynamical quark mass there is close to the smallest masses available at $\beta=5.6$ and 5.5. Therefore the errors introduced by our ''synthetic'' chiral extrapolation at $\beta=5.445$ do not appear to be large. However, the fact that the third data point in the fully unquenched analysis must be obtained in this way is another reason why we prefer the partially quenched analysis for the central values.

Figures 31 and 32 show the lattice spacing dependence of $f_B$ and $f_{B_s}/f_B$ after the fully unquenched chiral extrapolations. Like the partially quenched data of Figs. 22 and 24, the fully unquenched data are quite consistent with constant be-

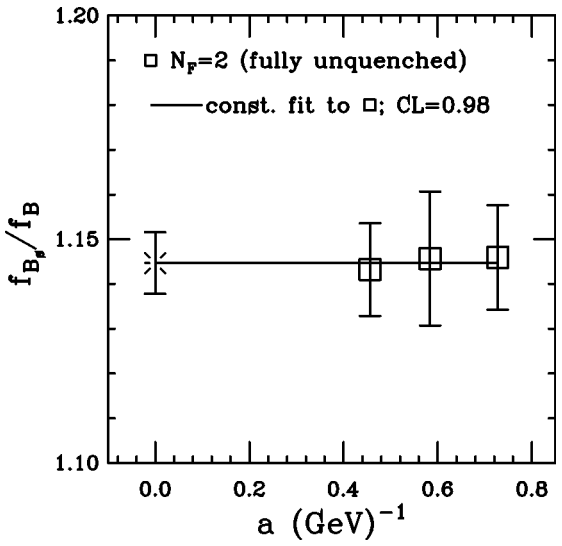


FIG. 32. Same as Fig. 31, but for $f_{B_s}/f_B$.

havior in $a$. The other decay constants and ratios behave similarly. The difference between the result of the constant fits in the fully unquenched and partially quenched cases is defined to be the systematic error of partial quenching, and is listed for the various quantities in Tables XI and XII. Given the issues in the fully unquenched analysis, we believe that this error determination is merely a rough estimate of the magnitude of the effect and do not take the sign of the difference seriously. We therefore symmetrize this error in the final error analysis.

### D. Rough estimate of chiral logarithm effects

As discussed in Sec. III E, our rather heavy-light mass values preclude a detailed study of chiral logarithms. However, an extrapolation of $f_{qq}/f_{Qq}$ (rather than individual decay constants), coupled with methods of determining $\kappa_s$ and $a^{-1}$ without significant chiral extrapolation, should provide an indication of the effect of the logarithms at light quark mass. Recall that, in the full theory, the coefficient of the chiral logs in $f_{qq}$ is probably larger than in $f_{Qq}$. This means that any errors in coming from a quadratic extrapolation of $f_{qq}/f_{Qq}$ should be opposite to those in our standard extrapolations of $f_{Qq}$ itself—especially for heavy-light decay constant ratios, which are less sensitive to the scale determination. In particular, the $f_{qq}/f_{Qq}$ approach should overestimate $f_{B_s}/f_B$, just as our standard approach may underestimate it. Indeed, the most significant change from the central value occurs in $f_{B_s}/f_B$ and is positive.

Table VI of Sec. III E shows the changes in the decay constants with various methods for fixing $\kappa_s$ and $a^{-1}$. Changes in the ratios are given in Table XIII. After eliminating the three lines in each table marked with asterisks (see Sec. III E), we average the changes in decay constants and ratios and find the standard deviations of the means. With the exception of the quantity $f_{D_s}/f_D$, the averages in all cases are positive and larger than the standard deviations of the means. We define the ''error due to chiral logarithm effects'' in these cases as the signed (positive) number that is the sum of the average and the standard deviation of the mean. This is slightly more conservative than just taking the straight average. For $f_{D_s}/f_D$, where the average is consistent with 0.00, we take the error as the (unsigned) standard deviation of the mean.

TABLE XIII. Estimates of the effects (in MeV) of chiral logarithms on the extrapolation of decay constant ratios. For descriptions of the methods, as well as $\kappa_s$ and $a^{-1}$, see Table VI in Sec. III E. Lines indicated by a ''*'' are eliminated from the averages.

| Method | $f_{B_s}/f_B$ | $f_{D_s}/f_D$ | $f_B/f_{D_s}$ | $f_{B_s}/f_{D_s}$ | $f_B/f_D$ |
|---|---|---|---|---|---|
| 1 | $+0.02$ | $+0.02$ | $+0.02$ | $+0.05$ | $+0.04$ |
| | $-0.02$ | $-0.09$ | $+0.07$ | $+0.01$ | $+0.00$ |
| 2 | $+0.06$ | $+0.06$ | $+0.01$ | $+0.06$ | $+0.06$ |
| | $+0.02$ | $-0.05$ | $+0.05$ | $+0.03$ | $+0.02$ |
| 3 | $-0.02$ | $-0.03$ | $+0.04$ | $+0.03$ | $+0.01$ |
| | $-0.07$ | $-0.13$ | $+0.08$ | $-0.00$ | $-0.02$ |
| 4 | $+0.04$ | $+0.04$ | $+0.02$ | $+0.06$ | $+0.05$ |
| | $+0.01$ | $-0.06$ | $+0.06$ | $+0.02$ | $+0.01$ |
| 5 | $+0.08$ | $+0.08$ | $+0.00$ | $+0.07$ | $+0.07$ |
| | $+0.05$ | $-0.03$ | $+0.04$ | $+0.04$ | $+0.03$ |
| 6 | $+0.03$ | $+0.03$ | $+0.03$ | $+0.06$ | $+0.05$ |
| | $+0.04$ | $-0.03$ | $+0.06$ | $+0.06$ | $+0.05$ |
| 7 | $+0.05$ | $+0.05$ | $+0.01$ | $+0.06$ | $+0.05$ |
| | $+0.07$ | $-0.00$ | $+0.05$ | $+0.06$ | $+0.05$ |
| 8 | $-0.01$ | $-0.02$ | $+0.04$ | $+0.04$ | $+0.03$ |
| | $+0.01$ | $-0.07$ | $+0.08$ | $+0.05$ | $+0.04$ |
| 9 | $+0.05$ | $+0.05$ | $+0.02$ | $+0.06$ | $+0.06$ |
| | $+0.06$ | $-0.01$ | $+0.05$ | $+0.06$ | $+0.06$ |
| 10 | $+0.07$ | $+0.08$ | $+0.00$ | $+0.06$ | $+0.06$ |
| | $+0.08$ | $+0.02$ | $+0.04$ | $+0.06$ | $+0.06$ |
| * 11 | $+0.12$ | $+0.15$ | $-0.01$ | $+0.10$ | $+0.11$ |
| * | $+0.18$ | $+0.18$ | $-0.02$ | $+0.11$ | $+0.11$ |
| 12 | $+0.02$ | $+0.01$ | $+0.02$ | $+0.06$ | $+0.03$ |
| * | $+0.17$ | $+0.15$ | $-0.01$ | $+0.09$ | $+0.10$ |
| **average** | $+0.03$ | $-0.00$ | $+0.04$ | $+0.05$ | $+0.04$ |
| **stand. dev. of mean** | 0.01 | 0.01 | 0.01 | 0.00 | 0.01 |

The chiral logarithm effects, while quite significant in the case of $f_{B_s}/f_B$ and some of the other ratios, appear to be considerably smaller than has been anticipated in Refs. [8,9]. We believe this due to the fact that we set the scale in our central values using $f_\pi$ and extrapolate the light-light and heavy-light decay constants in the same manner. Thus, much of the chiral logarithm effects, which are similar in $f_\pi$ and $f_B$, cancel.

On the other hand, we emphasize that our estimate of the chiral logarithm effects is, for a variety of reasons, rather rough. First of all, the changes in the decay constants and ratios vary a great deal among the different methods and

configurations shown in the tables. Indeed, the standard deviation (as opposed to the standard deviation of the mean) of a change is typically the same size as the average change and is sometimes larger. Secondly, our approach relies on $\chi$PT to find the quantities $m_{ss}$ and $f_{ss}$, and $\chi$PT is not necessarily rapidly convergent for *s* quarks. We have also performed only a partially quenched analysis of this issue. Because of the size of the errors, we have not attempted to extrapolate the dynamical quarks to their physical masses. Finally, we note that there is an inherent (though presumably small) inconsistency in our determinations of $\kappa_s$ and $a^{-1}$, which indirectly use the physical values of $f_\pi$, $f_K$, $m_\pi$ and $m_K$ (or $m_\eta$ or $m_\phi$). We cannot force all these quantities to have their physical values at once in a theory without a dynamical strange quark. For this reason, it is unclear for example whether it is better to use $N_f=2$ or $N_f=3$ PQ$\chi$PT in finding $f_{ss}$; we hope that our range of methods gives a reasonable range of results.

Given the crude nature of the chiral log error, we believe that it would be inappropriate at this stage to use the computations described in Sec. III E to correct our central values. Instead, we use them only for error estimates.

### E. Final error estimates and results

The magnetic mass error in Tables XI and XII is estimated with almost the same method as we used for the quenched calculation. The only difference is that here all the valence quarks are of Wilson type, so that there is no reduction of the magnetic mass error in the final error budget for the relative number of Wilson and clover estimates. The perturbative and $1/M$ fit errors in the tables are determined in exactly the same manner as in the quenched approximation.

The errors due to finite volume are studied by comparing results on sets R and G, both of which have $\beta=5.6$ and $am=0.01$, but which have spatial volumes $24^3$ and $16^3$, respectively. Note that all but one of our $N_f=2$ sets are large (spatial size $\sim$2.1–3.3 fm); only set G is comparable in size ($\sim$1.4 fm) to the quenched lattices. The difference between sets R and G is therefore likely to be a considerable overestimate of the actual finite volume error. Despite this, the differences are almost never statistically significant. Here a ''significant difference'' is defined as one that is larger than the sum, in quadrature, of the statistical errors of the two sets. When the difference is insignificant, we set the finite volume error to zero, as indicated in Tables XI and XII by the notation ''$\rightarrow$0.0.'' The only case where we find a significant ($\sim 1.6\sigma$) effect is in $f_{D_s}/f_D$.

The total systematic error *within* the current approximation (partially quenched $N_f=2$ theory) is then taken to be the sum of all the systematic errors above the line in Tables XI and XII: continuum extrapolation, valence chiral extrapolation, perturbative, magnetic mass, $1/M$ fit, and finite volume errors. Since these errors show no evidence of correlations, we perform the sum in quadrature. We do, however, treat positive and negative errors separately, since the valence chiral extrapolation error represents a binary choice and has a well determined sign.

We still need to estimate the error *of* the partially quenched $N_f=2$ approximation. One measure of this error has already been discussed: the partial quenching error. The effect of the missing third light virtual quark (the *s* quark) is estimated in a direct way by assuming a simple linear dependence of the decay constants on the number of dynamical flavors. The error is thus chosen to be one half the difference of the $N_f=2$ and quenched calculations. This estimate is labeled ''missing dynamical *s* quark'' in Tables XI and XII. We also estimate the effect in two indirect ways: by determining the change in the results when (i) the scale is fixed by $m_\rho$ (instead of $f_\pi$), and (ii) for strange quark quantities, when $\kappa_s$ is fixed by the vector meson sector ($m_\phi$) instead of the pseudoscalars. In full QCD (and with no other systematic errors), these differences should vanish, so their size is an estimate of the distance we are from the full theory.

The total error of the partially quenched $N_f=2$ approximation is then defined to be the maximum of the four estimates below the line in Tables XI and XII: partial quenching, scale, $\kappa_s$, and missing dynamical *s* quark. The latter three estimates have a well-determined sign, and we therefore find the maximum positive and maximum negative error separately. (As discussed above, the partial quenching error is treated symmetrically.) For the individual decay constants, the scale and missing dynamical *s* quark estimates are always largest; while the errors in the ratios are almost always dominated by the partially quenched error.

Finally we include an additional error due to the fact that our extrapolations from rather large light quark masses cannot see the chiral logarithms directly. This error is estimated in Sec. V D. We emphasize that it is necessarily crude.

Our final results for heavy-light decay constants, including the effects of dynamical quarks, are

$$f_B = 190(7)\left(^{+24}_{-17}\right)\left(^{+11}_{-2}\right)\left(^{+8}_{-0}\right)\ \text{MeV},$$

$$f_{B_s} = 217(6)\left(^{+32}_{-28}\right)\left(^{+9}_{-3}\right)\left(^{+17}_{-0}\right)\ \text{MeV},$$

$$f_D = 215(6)\left(^{+16}_{-15}\right)\left(^{+8}_{-3}\right)\left(^{+4}_{-0}\right)\ \text{MeV},$$

$$f_{D_s} = 241(5)\left(^{+27}_{-26}\right)\left(^{+9}_{-4}\right)\left(^{+5}_{-0}\right)\ \text{MeV},$$

$$\frac{f_{B_s}}{f_B} = 1.16(1)(2)(2)\left(^{+4}_{-0}\right),$$

$$\frac{f_{D_s}}{f_D} = 1.14(1)\left(^{+2}_{-3}\right)(3)(1),$$

$$\frac{f_B}{f_{D_s}} = 0.79(2)\left(^{+5}_{-4}\right)(3)\left(^{+5}_{-0}\right),$$

$$\frac{f_{B_s}}{f_{D_s}} = 0.92(1)(6)(2)\left(^{+5}_{-0}\right),$$

$$\frac{f_B}{f_D} = 0.91(2)\left(^{+6}_{-5}\right)\left(^{+2}_{-1}\right)\left(^{+5}_{-0}\right). \tag{46}$$

Here the errors are, respectively, statistical, systematic within the $N_f=2$ partially quenched approximation, the systematic errors of that approximation (due to partial quenching and the missing virtual strange quark), and an estimate of the effect of chiral logarithms.

The result for $f_{D_s}$ is consistent with experimental results; Ref. [63] obtains $f_{D_s^+}=280(19)(28)(34)$ MeV, which the *Review of Particle Physics* cites as ''the best and most recent value'' [64]. Our $N_f=2$ values are consistent with recent results of CP-PACS [65] and preliminary results of JLQCD [10], though our central values of the decay constants and ratios $f_{B_s}/f_B$ and $f_{D_s}/f_D$ are somewhat lower than those of CP-PACS.

## VI. CONCLUSIONS AND FUTURE DIRECTIONS

Equation (46) and Tables XI, XII, VI and XIII summarize our results. Chiral extrapolation, continuum extrapolation and perturbation theory are generally the biggest sources of errors for the decay constants, while partially quenching, the missing *s* quark, and the magnetic mass are also important for many of the ratios. Because the lattices $u,d$ have necessarily been rather heavy, as they have in other lattice calculations to date, the effects of chiral logarithms at low quark mass have only been investigated crudely and indirectly. We believe that is the error over which we have the least control at present.

Work in progress [45] addresses many of the above issues. Improved actions have decreased the continuum extrapolation errors significantly, as well as eliminated the separate magnetic mass error. A dynamical *s* quark is now explicitly included. Further, since the computations use a wide range of both dynamical and light valence quark masses, we hope to treat the chiral logarithms explicitly within a partially quenched framework [55,66]. This should provide more direct evidence about the issue of the size of chiral logarithm effects [8,9], as well as eliminate the explicit partial quenching error.

Future calculations will use staggered light quarks, as have already been investigated in conjunction with NRQCD heavy quarks [67]. This will allow for very light valence masses and therefore make possible a detailed study of chiral logarithms. To improve the chiral extrapolations still more, one-loop chiral perturbation theory calculations that take into account staggered taste[13] violation will be needed. Such calculations for pseudoscalar meson masses already exist; those for heavy-light decay constants are in progress [68].

The next step after that is likely to involve perturbation theory. Once the other errors have been reduced, the errors of one-loop perturbative calculations will no longer be acceptable. Higher order calculations using automated methods [69] or nonperturbative computations will be required.

## ACKNOWLEDGMENTS

We thank the HEMCGC Collaboration for use of lattice set G, and K.-I. Ishikawa for sharing unpublished results. This work was supported by the U.S. Department of Energy under contracts DOE–DE-FG02-91ER-40628, DOE–DE-FG03-95ER-40894, DOE–DE-FG02-91ER-40661, DOE–DE-FG02-97ER-41022 and DOE–DE-FG03-95ER-40906 and National Science Foundation grants NSF–PHY99-70701 and NSF–PHY00-98395. Calculations for this project were performed at Oak Ridge National Laboratory Center for Computational Sciences, San Diego Supercomputer Center, Indiana University, National Center for Supercomputing Applications, Pittsburgh Supercomputer Center, Maui High Performance Computing Center, Cornell Theory Center, CHPC (University of Utah), and Sandia National Laboratory.

[13]We prefer the term ''taste'' for the quantum number introduced by doubling in order to distinguish it from physical flavor.

[1] See, for instance, R. A. Briere *et al.*, ''CLEO-c and CESR-c: A New Frontier of Weak and Strong Interactions,'' CLNS report 01/1742 (revised 10/01); I. Shipsey, hep-ex/0203033.
[2] C. Bernard *et al.*, Nucl. Phys. B (Proc. Suppl.) **94**, 346 (2001).
[3] C. Bernard, Nucl. Phys. B (Proc. Suppl.) **94**, 159 (2001).
[4] C. Bernard *et al.*, Phys. Rev. Lett. **81**, 4812 (1998).
[5] C. Bernard *et al.*, Nucl. Phys. B (Proc. Suppl.) **42**, 388 (1995); **47**, 459 (1996); **53**, 358 (1997); **60A**, 106 (1998); **63**, 362 (1998); **73**, 372 (1999); in *Twenty Beautiful Years of Bottom Physics*, edited by R. A. Burnstein, D. M. Kaplan, and H. A. Rubin, AIP Conf. Proc. No. 424 (AIP, Woodbury, NY, 1998).
[6] A. El-Khadra, A. Kronfeld, and P. Mackenzie, Phys. Rev. D **55**, 3933 (1997).
[7] M. Lüscher *et al.*, Nucl. Phys. **B491**, 323 (1997); **B491**, 344 (1997).
[8] A. Kronfeld and S. Ryan, Phys. Lett. B **543**, 59 (2002).
[9] N. Yamada, review talk presented at the International Symposium, *Lattice 2002*, Boston, 2002 [Nucl. Phys. B (Proc. Suppl.) (in press)].
[10] N. Yamada *et al.*, Nucl. Phys. B (Proc. Suppl.) **106-107**, 397 (2002).
[11] C. Bernard and T. DeGrand (in preparation). See Ref. [3] for a brief discussion of the calculation.
[12] C. Bernard *et al.*, Nucl. Phys. B (Proc. Suppl.) **83-84**, 289 (2000).
[13] B. Sheikholeslami and R. Wohlert, Nucl. Phys. **B259**, 572 (1985).
[14] G.P. Lepage and P.B. Mackenzie, Phys. Rev. D **48**, 2250 (1993).
[15] C. Bernard, J. Labrenz, and A. Soni, Phys. Rev. D **49**, 2536 (1994).
[16] K.C. Bowler *et al.*, Nucl. Phys. **B619**, 507 (2001).
[17] S. Aoki *et al.*, Phys. Rev. Lett. **80**, 5711 (1998).
[18] Y. Kuramashi, Phys. Rev. D **58**, 034507 (1998).
[19] K. Bitar *et al.*, Phys. Rev. D **48**, 370 (1993); T. Klassen, *ibid.* **51**, 5130 (1995).
[20] While the current paper was being written, a calculation of the renormalizations and $q^*$ values for bilinears with Wilson and

clover fermions appeared: J. Harada *et al.*, Phys. Rev. D **65**, 094513 (2002). The choices of $q^*$ in the current paper and the results of Ref. [11] are compatible with those in Harada *et al.* Note, however, that in the clover case (Sec. II B) we estimate the heavy-light $q^*$ from the static-light $q^*$ with the appropriate values of $c_{SW}$ for our lattices ($c_{SW}=1.769$ and 1.644), while Harada *et al.* quote values for the heavy-light case with $c_{SW}=1$.

[21] C. Bernard, M. Golterman, and C. McNeile, Phys. Rev. D **59**, 074506 (1999).
[22] O. Hernandez and B. Hill, Phys. Rev. D **50**, 495 (1994).
[23] E. Eichten and B. Hill, Phys. Lett. B **240**, 193 (1990).
[24] Ph. Boucaud, C.L. Lin, and O. Pène, Phys. Rev. D **40**, 1529 (1989); **41**, 3541(E) (1990).
[25] M. Guagnelli *et al.*, Nucl. Phys. **B595**, 44 (2001).
[26] T. Bhattacharya *et al.*, Phys. Rev. D **63**, 074505 (2001).
[27] S. Sint and P. Weisz, Nucl. Phys. **B502**, 251 (1997).
[28] K.-I. Ishikawa, T. Onogi, and N. Yamada, Nucl. Phys. B (Proc. Suppl.) **83-84**, 301 (2000).
[29] K.-I. Ishikawa and T. Onogi (private communication).
[30] D. Becirevic *et al.*, Nucl. Phys. **B618**, 241 (2001).
[31] The result without the $d_1$ term was kindly made available to us by K.-I. Ishikawa.
[32] A. Kennedy and B. Pendleton, Phys. Lett. **145B**, 393 (1985); N. Cabibbo and E. Marinari, *ibid.* **119B**, 387 (1982).
[33] M. Creutz, Phys. Rev. D **36**, 515 (1987); F.R. Brown and T.J. Woch, Phys. Rev. Lett. **58**, 2394 (1987).
[34] S. Gottlieb, W. Liu, D. Toussaint, R.L. Renken, and R.L. Sugar, Phys. Rev. D **35**, 2531 (1987).
[35] HEMCGC Collaboration, K.M. Bitar *et al.*, Phys. Rev. D **49**, 6026 (1994).
[36] D. Henty and R. Kenway, Phys. Lett. B **289**, 106 (1992).
[37] A. Duncan, E. Eichten, and H. Thacker, Nucl. Phys. B (Proc. Suppl.) **30**, 441 (1993).
[38] T. Draper and C. McNeile, Nucl. Phys. B (Proc. Suppl.) **34**, 453 (1994).
[39] H. van der Vorst, SIAM (Soc. Ind. Appl. Math.) J. Sci. Stat. Comput. **13**, 631 (1992).
[40] B. Thacker and G.P. Lepage, Phys. Rev. D **43**, 196 (1991); G. Kilcup, Nucl. Phys. B (Proc. Suppl.) **34**, 350 (1994); C. Michael, Phys. Rev. D **49**, 2616 (1994).
[41] H. H. Harmon, *Modern Factor Analysis*, 2nd ed. (University of Chicago Press, Chicago, 1967), Chap. 8.
[42] A. Anastassov *et al.*, Phys. Rev. D **65**, 032003 (2002).
[43] I.W. Stewart, Nucl. Phys. **B529**, 62 (1998).
[44] A. Abada *et al.*, Phys. Rev. D **66**, 074504 (2002).
[45] C. Bernard *et al.*, Nucl. Phys. B (Proc. Suppl.) **106-107**, 412 (2002); and work in progress.
[46] J.L. Goity, Phys. Rev. D **46**, 3929 (1992); B. Grinstein *et al.*, Nucl. Phys. **B380**, 369 (1992).
[47] J. Gasser and H. Leutwyler, Nucl. Phys. **B250**, 465 (1985).
[48] S. Sharpe, Phys. Rev. D **56**, 7052 (1997).
[49] S. Sharpe and N. Shoresh, Phys. Rev. D **62**, 094503 (2000).
[50] H. Leutwyler, Phys. Lett. B **378**, 313 (1996).
[51] S. Hashimoto *et al.*, Phys. Rev. D **66**, 014503 (2002).
[52] See, for example, H. Georgi, in *Perspectives in the Standard Model*, Proceedings of TASI 91, Boulder, Colorado, 1991, edited by R. K. Ellis *et al.* (World Scientific, Singapore, 1992); B. Grinstein, in *High Energy Phenomenology*, Proceedings of the Workshop on High Energy Phenomenology, Mexico City, 1991, edited by M. A. Péres and R. Huerta (World Scientific, Singapore, 1992); N. Isgur and M. B. Wise, in *Heavy Flavors*, edited by A. J. Buras and M. Lindner (World Scientific, Singapore, 1992); M. Neubert, Phys. Rep. **245**, 259 (1994).
[53] M.B. Voloshin and M.A. Shifman, Yad. Fiz. **45**, 463 (1989); H.D. Politzer and M.B. Wise, Phys. Lett. B **206**, 681 (1988).
[54] A. El-Khadra *et al.*, Phys. Rev. D **58**, 014506 (1998).
[55] S. Sharpe and Y. Zhang, Phys. Rev. D **53**, 5125 (1996); M. Booth, *ibid.* **51**, 2338 (1995).
[56] S. Sharpe, Phys. Rev. D **46**, 3146 (1992); C. Bernard and M. Golterman, *ibid.* **46**, 853 (1992).
[57] M. Albanese *et al.*, Phys. Lett. B **192**, 163 (1987).
[58] C.W. Bernard and T. DeGrand, Nucl. Phys. B (Proc. Suppl.) **83-84**, 845 (2000).
[59] T. DeGrand, A. Hasenfratz, and T. Kovács, Nucl. Phys. **B547**, 259 (1999); T. Blum *et al.*, Phys. Rev. D **55**, R1133 (1997).
[60] C. Bernard *et al.*, Nucl. Phys. B (Proc. Suppl.) **83-84**, 274 (2000).
[61] M. Stephenson *et al.*, Phys. Rev. D **63**, 034501 (2001).
[62] Compare, for example, A. Hasenfratz and F. Knechtli, Phys. Rev. D **64**, 034504 (2001).
[63] M. Chada *et al.*, Phys. Rev. D **58**, 032002 (1998).
[64] Particle Data Group, D. Groom *et al.*, Eur. Phys. J. C **15**, 1 (2000), p. 395.
[65] A. Ali Khan *et al.*, Phys. Rev. D **64**, 034505 (2001).
[66] C. Bernard and M. Golterman, Phys. Rev. D **49**, 486 (1994).
[67] M. Wingate, Nucl. Phys. B (Proc. Suppl.) **106-107**, 379 (2002).
[68] C. Bernard, Phys. Rev. D **65**, 054031 (2002); C. Aubin *et al.*, talk presented to the International Symposium, *Lattice 2002* [9], hep-lat/0209066; C. Aubin and C. Bernard (in press).
[69] M. Nobes, H. Trottier, G.P. Lepage, and Q. Mason, Nucl. Phys. B (Proc. Suppl.) **106–107**, 838 (2002).